République Algérienne Démocratique et Populaire

Ministère de l'Enseignement Supérieur et de la Recherche Scientifique

Université A. MIRA - Bejaïa

Faculté des Sciences Exactes

Département de Chimie

جامعة بجاية
Tasdawit n Bgayet
Université de Béjaïa

Mémoire de Master

Présente par :

Ms Nayebare Praise

En vue de l'obtention du diplôme de Master en Chimie

Spécialité : Chimie Analytique

Thème :

Synthesis, characterisation by infrared spectroscopy, X-ray diffraction, TGA/DSC of coordination polymers and the study of their photo-luminescent properties

Soutenu le :

Devant le jury composé de :

Nom & Prénom	Département d'affiliation	Qualité
Mr Belabbas Imad	Chimie	Président
Mr Zidane Youcef	Chimie	Examinateur
Mme Belaid Sabrina	Chimie	Encadrant

2024-2025

Acknowledgments

First and foremost, I thank the Almighty God for His infinite mercy and grace, which have sustained me with strength and good health throughout this journey. Truly, all blessings, honour, glory, and power be unto the Almighty.

I extend my sincere thanks to Professor Belabbas Imad and Professor Zidane Youcef for graciously accepting to evaluate the quality of this work. I am honoured by your time and consideration.

I would like to express my deepest gratitude to my supervisor, Professor Sabrina Belaid, for giving me the opportunity to work under her guidance. Her constant support, invaluable advice, patience, and kindness have been instrumental in the completion of this work. Thank you, Madam, for always being available whenever I needed help it has been a great honour to be your student.

I am also sincerely grateful to my co-supervisors, Madam Maouche Roza and Madam Cheddani Yasmine, for their dedicated guidance, patience, and unwavering support throughout the preparation of this manuscript. Working under your supervision has truly been a rewarding experience.

My sincere thanks go to Professor Belkacem Benmerad, the laboratory technician Mr. Mekki Bouhali, and the entire management of LPCMC for their availability, technical assistance, and constant support that greatly contributed to the success of this research.

I would also like to thank the Department of Chemistry Laboratory for their hospitality and cooperation, as well as the CRAPC technical platform in Béjaïa for their warm welcome and assistance with the powder XRD measurements.

To my beloved family, friends, and everyone who has offered unwavering support throughout the course of this work, I am deeply grateful for your love, care, and encouragement.

Lastly, I extend my appreciation to myself for the hard work, resilience, and determination that enabled me to complete this study on time

Table of contents

List of abbreviations and symbols

- Cps: Coordination polymers
- Mofs: Metal Organic Frameworks
- Ln: Lanthanides
- TGA: Thermogravimetric Analysis
- La: Lanthanum
- Dy: Dysprosium
- Tb: Terbium
- Sm: Samarium
- Yb: Ytterbium
- Er: Erbium
- Gd: Gadolinium
- Pr: Praseodymium
- Nd: Neodymium
- pim: Pimelate ligand
- Ip: isophthalate ligand
- Uv: Ultra violet
- ° C: Degree Celsius
- u.a: arbitrary units
- pH: potential hydrogen
- λ: wave length
- ν: Stretching vibration frequency
- ν_{as}: asymmetric stretching vibration
- ν_{s}: symmetric stretching vibration
- δ: bending vibration
- IR: infrared
- XRD: X ray diffraction
- XR: X rays
- PXRD: powder X ray diffraction
- THF: Tetrahydrofuran

General Introduction

General Introduction

Coordination polymers (CPs) are an important class of crystalline materials formed by connecting metal ions with ligands through coordination bond. These connections can extend in one, two, or three dimensions, creating diverse structural frameworks [1]. Because of their flexible design and wide range of properties, CPs have become a major area of interest in materials chemistry and crystal engineering [2].

One of the most exciting features of CPs is how easily their structure and function can be tuned. By carefully choosing the metal ions, ligands, and reaction conditions, researchers can design materials with specific properties. This makes CPs useful for many applications, including gas storage, catalysis, magnetism, and biomedical uses[3]. Luminescent coordination polymers are being explored for use in sensors, light-emitting devices, anti-counterfeiting materials, and imaging [4,5].

Lanthanide ions (Ln^{3+}) are especially attractive for making luminescent CPs because they emit light with high colour purity and long lifetimes. However, their light-emitting transitions are weak on their own. To help with this, special ligands can be used to absorb energy and transfer it to the lanthanide this is known as the antenna effect[6].

In this study, we focus on the synthesis and characterization of lanthanide-based CPs using two specific dicarboxylic acid ligands: isophthalic acid and pimelic acid.

Isophthalic acid is a rigid, aromatic ligand with two carboxylic acid groups positioned at the 1,3-positions on a benzene ring. Its rigidity supports the formation of stable, extended structures, while its aromatic nature enables π-conjugation, which can enhance energy transfer to lanthanide centers making it particularly useful in luminescent materials. In addition, the spatial orientation of its functional groups allows for predictable coordination behaviour, which contributes to structural regularity in the resulting CPs[7].

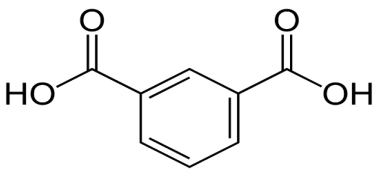

Isophthalic acid

Pimelic acid, on the other hand, is a flexible aliphatic ligand with a seven-carbon chain between its carboxylic acid groups. This flexibility allows it to adapt to different coordination environments, often acting as a spacer that facilitates the formation of extended frameworks[8].

General Introduction

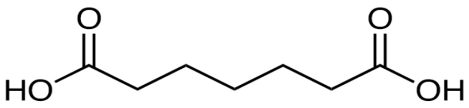

Pimelic acid

The aim of this work is to better understand how the combination of lanthanide metal ions and specifically chosen ligands affect the formation, structure, and properties of coordination polymers. Through this investigation, we aim to contribute to a deeper understanding of CP design and open up possibilities for future functional materials.

This work is divided into three chapters:

Chapter 1: coordination chemistry and rare earth metals

This chapter introduces the fundamental concepts of coordination chemistry and coordination polymers. It outlines the key characteristics of rare earth elements, with particular emphasis on their optical properties. Additionally, it highlights the advantages of rare earth-based coordination polymers and explores their potential applications.

Chapter 2: Materials and methods

This chapter presents the various synthesis methods used in the preparation of the coordination polymers studied in this manuscript. It also describes the characterization techniques employed to analyse and better understand the properties of these compounds. In addition, it introduces the main compounds used throughout this study.

Chapter 3: Results and discussion

This chapter begins with a literature review of lanthanide-based coordination polymers involving the ligands used in this study. It then presents the experimental synthesis procedures, followed by a detailed discussion of the results obtained.

This manuscript begins with a general introduction, which gives a brief view of the all the study carried out and concludes with a general summary encompassing all the work carried out, the results obtained throughout this project, as well as the perspectives for future development.

Chapter 1: Coordination chemistry and rare earth metal

Chapter 1: Coordination chemistry and rare earth metals

1.1 Coordination chemistry

1.1.1 History of coordination chemistry

During the first half of the 19th century, discoveries of coordination chemistry were few, sporadic and accidental until 1856, after Wolcott Gibbs and Frederick Genth 's classic memoire that chemists began to devote themselves in earnest to a systematic study of this field. Their study on metal-ammonia provided the foundational data that was later used to develop coordination theories

In 1893, Alfred Wener revolutionised inorganic chemistry by explaining the structure and bonding in coordination compounds. His key ideas were; primary (ionisable valence) and secondary (non-ionisable valence) and the coordination sphere concept [9].

According to Wener every metal in a particular oxidation state that is, with a particular primary valence, also has a definite coordination number, that is, a fixed number of secondary valences that must be satisfied. Now, whereas primary or ionizable valences can be satisfied only by anions, secondary or non-ionizable valences can be satisfied not only by anions but also by neutral molecules containing donor atoms such as nitrogen, oxygen, sulphur, and phosphorus The secondary valences are directed in space around the central metal atom, and when combined with donor atoms form a "complex" [10, 11].

Below in (**Figure 1. 1)** is the one the structure of amine cobalt (III) complex, one of the first complexes in Wener's discoveries.

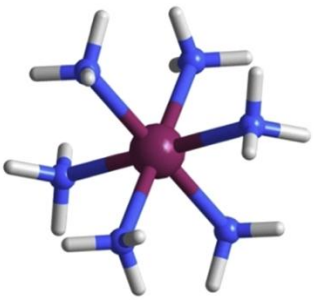

Figure 1. 1 The structure proposed by Werner for the ammine cobalt (III) complex [12].

Werner's contributions to coordination chemistry laid the foundations of broad areas of modern inorganic chemistry including stereochemistry, catalysis, solid-state chemistry, supramolecular

chemistry, nanotechnology, bioinorganic chemistry, metal-based pharmaceuticals, and even coordination polymers (CP) [11].

1.1.2 Coordination Complexes

1.1.2.1 Definition

In a coordination complex, a central atom or ion (electron acceptor) is joined to one or more molecules or ions (ligands/ electron donor) through coordinate bonds. Complexes can be neutral, positive or negatively charged. Examples of coordination complexes include, $[Fe(CN)_6]^{4-}$, $[Ni(CO)_4]$ [13].

Coordination complexes can be mononuclear if they contain only one central metal ion, binuclear if they contain two central metal ions or polynuclear if they have more than two metal ions [11].

1.1.2.2 Ligands

The term ligand originates from the Latin verb ligare, meaning "to bind." In coordination chemistry, ligands are ions or molecules that donate one or more pairs of electrons to a central metal atom or ion to form a coordination complex. This interaction occurs through a coordinate covalent bond (also known as a dative bond), where the ligand donates both electrons for the shared pair[14].

Ligands must possess at least one lone pair of electrons on a donor atom, typically nitrogen, oxygen, sulphur, or a halide. These electron-rich species stabilize metal ions by satisfying their coordination requirements and often influence the geometry, reactivity, and electronic properties of the resulting complexes[11].

Classification of ligands

Occasionally ligands can be cations (NO^+, $N_2H_5^+$), anions (F^-, Cl^-, Br^-, I^-, S_2^-, CN^-, NCS^-, OH^-, NH_2^-) or neutral (NH_3, H_2O, NO, CO).

On the basis of the number binding sites with the central metal atom, ligand can be classified into:

- Mono/Unidentate Ligands: They have one donor atom, i.e., they can donate only one electron pair to the central metal atom /ion e.g., F^-, Cl^- Br^- H_2 O, NH_3, CN^-, NO_2^- OH^-, CO etc [15].

- Bidentate Ligands: Ligands which have two donor atoms and have the ability to link with the central metal atom/ion at two positions are called bidentate ligands for example 1,10-phenanthroline (Phen) in (**Figure 1. 2**).

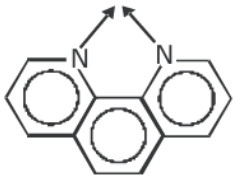

Figure 1. 2 structure of 1,10-phenanthroline (Phen).

- Polydentate or multidentate ligands; Ligands having more than two donor atoms are. Examples include;
  - ✓ Tridentate Ligands**:** These have three donor atoms for example 2 ,2' ,6' ,2"-Terpyridyl [13] in (**Figure 1. 3**).

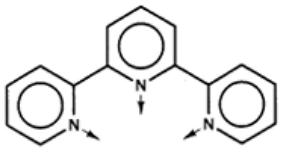

Figure 1. 3 Structure of 2 ,2' ,6' ,2"-Terpyridyl.

✓ Tetradentate Ligands: These ligands possess four donor atoms. For example, in (**Figure 1. 4**) Triethylenetetramine (Trien) [16].

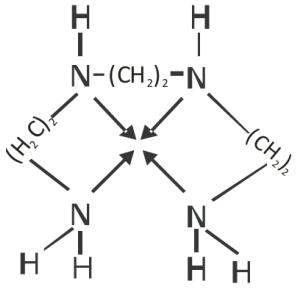

Figure 1. 4 Structure of Triethylenetetramine (Trien)

- Chelating ligand; Where the one ligand employs two different donors to attach to the same metal, we have a situation called chelation, a chelate ring has been formed. A chelate ring is defined formally as the cyclic system that includes the two donor atoms, the metal ion, and the part of the ligand frame work joining the two coordinated donors. [5].

Chelating ligands tend to form more thermodynamically stable complexes than equivalent monodentate ligands due to the entropy gain upon binding and the formation of the ring. (The entropy gain is associated with the displacement of multiple monodentate ligands by a single chelating ligand, resulting in a net increase in disorder). This is known as the chelate effect, which also contributes to increased inertness and decreased lability of metal complexes[17].

(Figure 1. 5) shows formation of a chelate ring by Diaminoethane, a molecule with two amine groups. Once the first lone pair is coordinated, the second lone pair from the other amine can be oriented in a direction more appropriate for bonding than is the case for two lone pairs on a single atom, with limited bond angle distortion permitting both to coordinate, illustrated at right, in a chelated coordination mode [11].

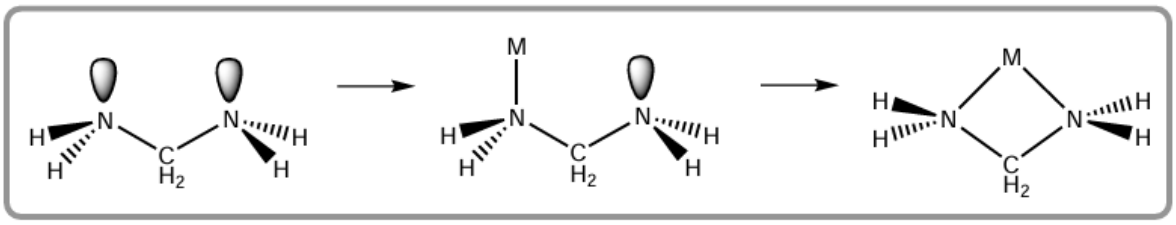

Figure 1. 5 formation of a chelate ring.

- Ambidentate ligands: These ligands have two or more donor atoms but in forming complexes, only one donor atom is attached to the metal/ion. An example of such ligands is the thiocyanate ion (NSC^-) which can attach to the metal atom either by the N atom to give a thiocyanato – M– N complex or by the S atom to give a thiocyanato – M–S complex. [13, 16].
- Bridging ligands; These Ligands can accommodate more than one metal ion in two distinct ways; by using two different donor atoms on one ligand to bind to two separate metal ions; or by using two different lone pairs on the same donor group to bind to two separate metal ions. The former leads to greater distance between the like-charged metal centres, and is thus likely to be a less demanding process. The latter brings the metal ions much closer together but can only occur, of course, with donor groups that have the potential to provide at least two lone pairs, and that are usually anionic so as to help two like-charged metal centres approach each other closely[11, 13, 14].

  The (**Figure 1. 6**) below explains how ammonia acts as a bridging ligand. Ammonia coordinates as a monodentate ligand to one metal. When a proton is removed it exhibits the capacity to attach the resultant additional lone pair to a second metal ion in a bridging

mode efficiently to two metal ions. Bridging ligands are critical in the formation of coordination polymers, supramolecular assemblies, and metal-organic frameworks (MOFs) [16]

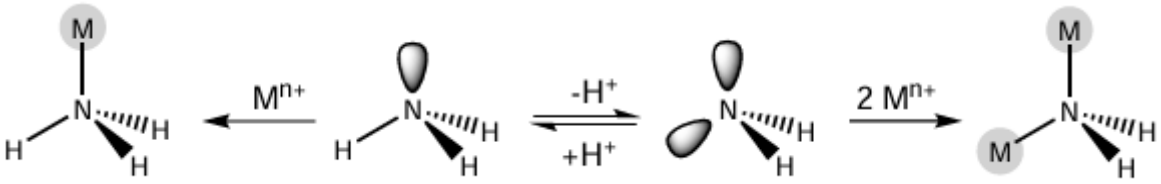

Figure 1. 6 ammonia as a bridging ligand.

1.1.2.3 Coordination bonds

The coordinate bond / dative bond or coordinate covalent bond is between the central metal ion and the ligand. The bonding electrons are supplied by the ligand unlike in the typical covalent bond where each atom contributes one electron. For example, in $[Co\ (NH_3)_6]^{3+}$ each NH_3 donates its pair of electrons to Co^{3+}[11].

In (**Figure 1. 7**) H_3B and Ag^+ act as a metalloid (the electron-pair acceptors), NH_3 is the species providing the electron pair (the electron-pair donor) to form a coordinate bond.

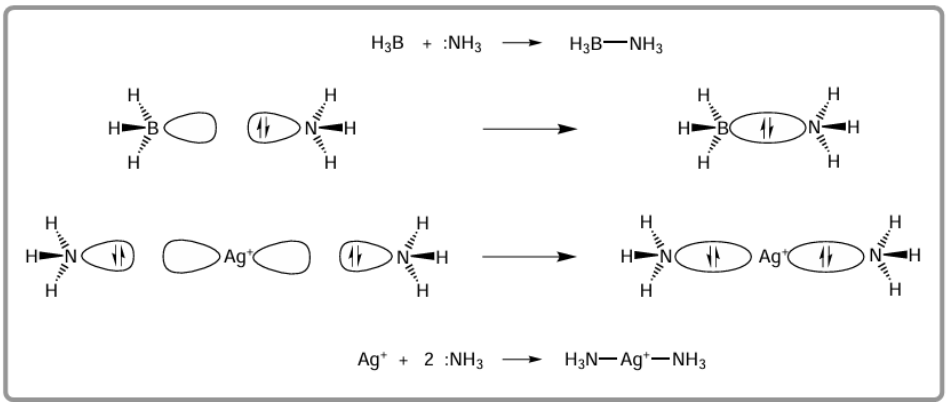

Figure 1. 7 a schematic view of the formation of a coordinate bond[16].

1.1.2.4 Coordination sphere

A coordination sphere refers to the central metal ion in a coordination compound along with all the ligands (atoms, ions, or molecules) that donate electron pairs to the metal. The primary coordination sphere consists of ligands that are directly attached to the metal through coordinate bonds. This sphere is usually enclosed in square brackets when writing the chemical formula.

Secondary coordination sphere includes molecules or ions that are not directly bonded to the metal but are associated through hydrogen bonding, weak electrostatic forces or Vanderwal's forces of attraction. The ionisable groups are written outside the bracket and are termed as counter ions. For example, in the complex $k_4[Fe(CN)_6]$, $[Fe(CN)_6]^{4-}$is the primary coordinate sphere and the secondary coordinate sphere is K^+[11, 14, 16].

1.1.2.5 Coordination numbers

The coordination number (C.N.) of a metal atom/ion in a complex is the total number of electron pairs accepted by central metal atom/ion from ligands through coordinate bond. The coordination number varies between 2 and 12 depending on the nature of the central atom and the ligand [13].

1.1.2.6 Geometrical structures of complexes

The geometrical structures of metal complexes can be determined in ways. When single crystals of a compound are grown, X-ray diffraction is the gold standard, it gives 3D structures with exact position of atoms, shapes, bond distances, and bond angles. Other methods include; Nuclear magnetic resonance, mass spectroscopy etc [17].

The spatial arrangement of the ligand atoms which are directly attached to the central atom/ion defines the coordination polyhedron. The coordination polyhedron depends on; the coordination number, steric effects of the ligand, the size and the electronic configuration of the metal ion. The most common coordination polyhedral are octahedral, square planar and tetrahedral [13, 17].

1.1.3 Coordination polymers

1.1.3.1 History

The coordination polymer synthesized was "Prussian Blue" (it is a pigment blue with chemical formular $Fe_7(CN)_{18}(H_2O)_x$, used medicinally in the treatment of cesium and thalium poisoning). This compound was discovered accidentally by Johann Jacob Diesbach at the beginning of the seventeenth century[18]. The first coordination polymer was discovered by J.C. Bailar (American chemist) in 1964 when he compared organic polymers to inorganic species that can be considered as polymer species[19].

The current extensive interest in coordination polymers was triggered after the reports of Robson and Hoskins. They proposed that the new materials with interesting properties such

porosity and catalysis could be deliberately engineered through describing crystal structures in terms of nets [18].

1.1.3.2 Definition

Coordination polymer is a solid-state structure with repeating coordination entities extending in one, two or three dimensions (1D, 2D or 3D). CPs are assembled by metal ions and bridging organic ligands, and sometimes with additional supramolecular interactions, into highly ordered 3D solid structures [12, 18].

Coordination polymers in which metal ions are linked by organic ligands into structures with potential voids are often referred to as metal-organic frameworks (MOFs) or porous coordination polymers. The topology of coordination polymers can be tuned almost at will by careful choice of metal ions and organic ligands and a nearly infinite variety of structures can be obtained [20].

1.1.3.3 Types coordination polymers

Coordination polymers can be classified according to their dimension into the 1D (mono dimensional), 2D (bidimensional) and the 3D (Tri dimensional) as seen in **Table 1. 1** below [18].

Table 1. 1 coordination polymers based on their dimensionality.

Dimensionality	**1D**	**2D**	**3D (MOFS)**
Description	Linear or zig-zag metal-ligand repeating units forming infinite chains. They can be formed by simple bridging ligands like Cl^-, CN^-, or organic ligands like carboxylates[21]	Metal centers connected in planar grids or honeycomb patterns. Ligands bridge in two directions, forming sheet-like networks. These sheets may be stack with π–π interactions,	Frame works where metal nodes and linkers extend in three dimensions. Known as Metal–Organic Frameworks (MOFs) when the network is crystalline and porous.[2]

		hydrogen bonding, or van der Waals forces[19].	
Common structures	• zigzag chains 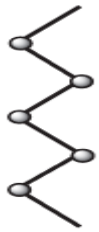 • helical • ladder	• Rectangular • brick-wall structures • Honey comb 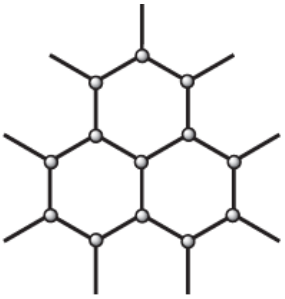	• cubic • Diamondoid (Dia) 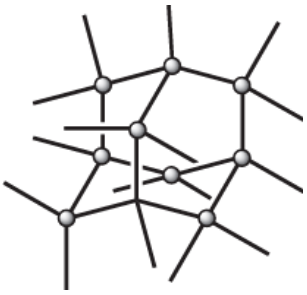

Below in (**Figure 1. 8**), (**Figure 1. 9**), and (**Figure 1. 10**) are examples of each of the three types of coordination polymers illustrated in the table above.

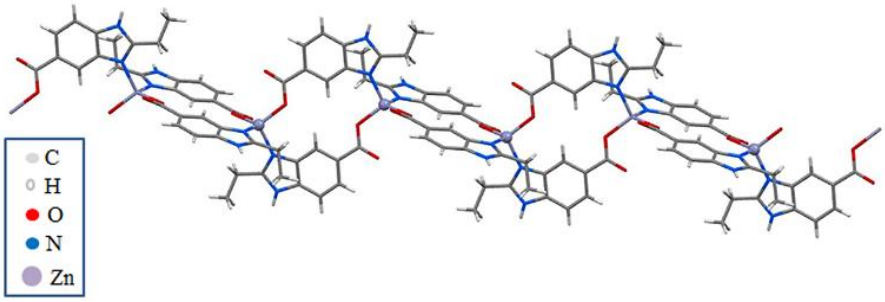

Figure 1. 8 An example of 1 D Coordination polymer[22].

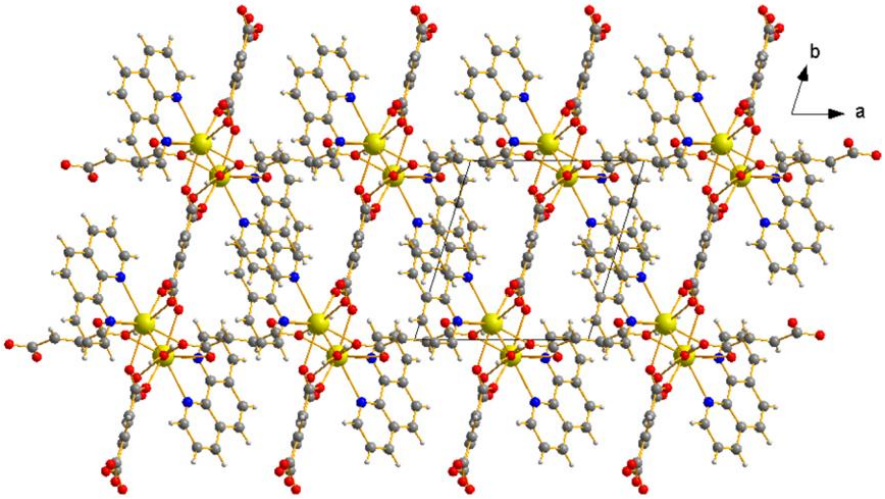

Figure 1. 9 an example of a 2 D coordination polymer[23].

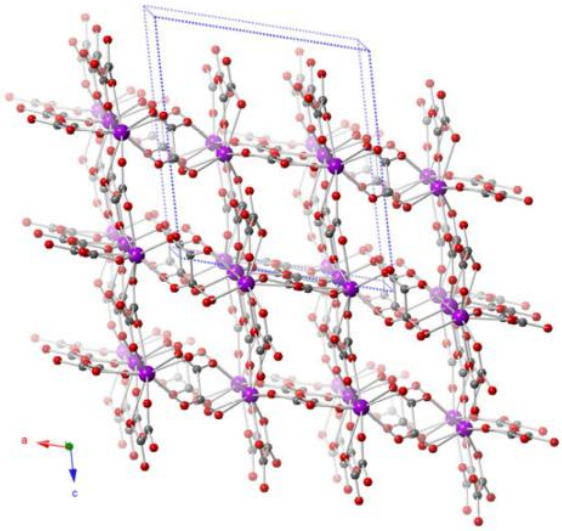

Figure 1. 10 An example of 3 D coordination polymer[24].

1.2 Lanthanides (the rare earth elements)

1.2.1 History and definition

The series of 15 elements of the periodic table from lanthanum (57) to lutetium (71) is commonly referred to as lanthanides or 4f-elements (Ln). When scandium and yttrium are added, the series takes the name of "rare earths"[25].

The first rare-earth element, yttrium, was discovered by the Finnish chemist Johan Gadolin in 1794 from a mineral now named gadolinite near Ytterby (Sweden). It took more than 100 years

(1803–1907) to identify the remaining naturally occurring elements from minerals whereas radioactive Promethium (pm) was synthesized in 1947 [26].

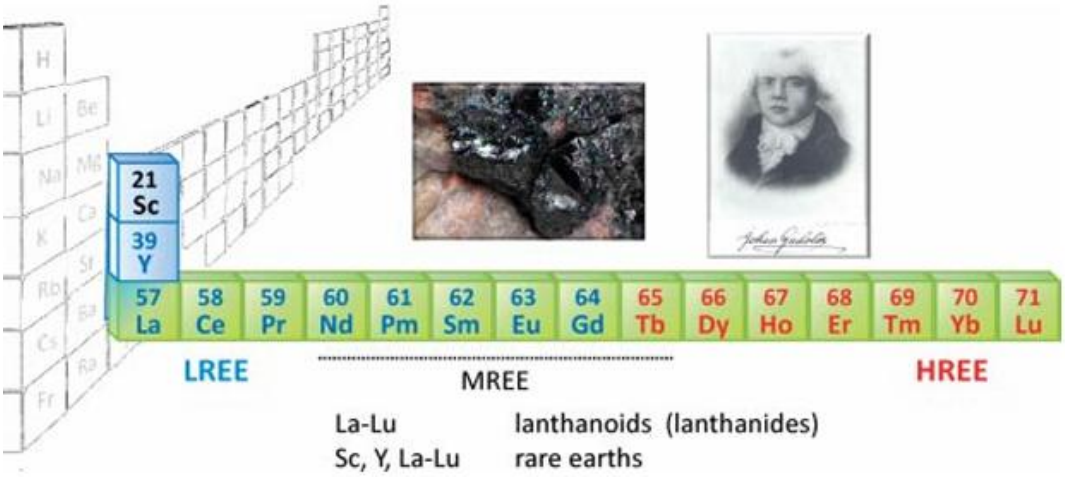

Figure 1. 11 Position of the lanthanoids (lanthanides) and rare earths in the Periodic Table with picture of the black stone of Ytterby from which yttrium oxide was isolated and the portrait of Johan Gadolin [25].

1.2.2 Occurrence of lanthanides

Rare earth elements are distributed broadly in the Earth's crust in relatively small concentrations as their name "rare" suggests with Cerium, the most abundant while Promethium, best known as an artificial element, occurs in very minute quantities in natural materials because it has no stable or long-lived isotopes. Lanthanide elements with low atomic numbers are generally more abundant in the earth's crust than those with high atomic numbers. Those with even atomic numbers are two to seven times more abundant than adjacent lanthanides with odd atomic numbers as observed in **(Table 1. 2)** [27].

Table 1. 23 REEs, atomic numbers, and abundances.

Element	**Symbol**	**Atomic number**	**Abondance(ppm)**
Yttrium	Y	39	22
Lanthanum	La	56	30
Cerium	Ce	58	64
Praseodymium	Pr	59	7.1
Neodymium	Nd	60	26

Promethium	Pm	61	Not available
Samarium	Sm	62	4.5
Europium	Eu	63	0.88
Gadolinium	Gd	64	3.8
Terbium	Tb	65	0.64
Dysprosium	Dy	66	3.5
Holmium	Ho	67	0.80
Erbium	Er	68	2.3
Thulium	Tm	69	0.33
Ytterbium	Yb	70	2.2
Lutetium	Lu	71	0.32

1.2.3 Properties of rare earth elements

1.2.3.1 Electronic configuration

According to the principle of lowest energy, there are two types of electronic configurations for the lanthanide elements: [Xe] $4f^n$ $6s^2$ and [Xe] $4f^{(n-1)}$ $5d^1$ $6s^2$; n represents a number from 1 to 14 and [Xe] represents the electronic configuration of xenon which is $1s^2$ $2s^2$ $2p^6$ $3s^2$ $3p^6$ $3d^{10}$ $4s^2$ $4p^6$ $4d^{10}$ $5s^2$ $5p^6$ [28].

At lanthanum, the 5d subshell is lower in energy than 4f, so lanthanum has the electron configuration [Xe] $6s^2$ $5d^1$. As more electrons are added to the nucleus, the 4f orbitals contract rapidly and become more stable than the 5d (the 4f orbitals penetrate the 'xenon core' more). As a result of this, Ce has the electron configuration [Xe] $6s^2$ $5d^1$ $4f^1$ and the trend continues with Pr having the arrangement [Xe] $6s^2$ $4f^3$. This pattern continues for the metals Nd–Eu, all of which have configurations [Xe] $6s^2$ $4f^n$ (n = 4–7) [28].

After Europium, the 4f subshell in Gd is half filled (more stable) such that the next electron is added to the 5d orbital thus Gd being [Xe] $6s^2$ $5d^1 4f^7$. However, the electron configuration pattern of [Xe] $6s^2$ $4f^n$ (n = 9–14) f is resumed from Tb to Yb. The last lanthanide, lutetium, where the 4f subshell is now filled, is predictably [Xe] $6s^2$ $5d^1 4f^{14}$ [29].

1.2.3.2 The valence state of rare earth elements

The metal reactivity of rare earth metals increases gradually from scandium to lanthanum and decreases gradually from lanthanum to lutetium. That is to say, lanthanum is the most reactive metal of the 17 rare earth elements.

According to Hund's rule, electron shells are stable when empty, full or half-full. For example, the configurations $4f^0$ (La^{3+}), $4f^7$ (Gd^{3+}), and $4f^{14}$ (Lu^{3+}) are stable. Ce^{3+}, Pr^{3+} and Tb^{3+} have one or two more electrons than required for stable electronic configurations so they can be further oxidized to a 4^+ state. In contrast, Sm^{3+}, Eu^{3+}, and Yb^{3+} have one or two less electrons than required for a stable electronic configuration and they, therefore, tend to receive one or two electrons and undergo a reduction to a 2+ state a reduction to a 2+ state as illustrated in **Table 1. 3** [27, 30].

Table 1. 3 Electron configurations of the lanthanides and their common ions [22].

Symbol	**Electronic configuration**	**Ln^{+3}**	**Ln^{+4}**	**Ln^{+2}**
La	[Xe] $5d^1$ $6s^2$	[Xe]		
Ce	[Xe] $4f^1$ $5d^1$ $6s^2$	[Xe] $4f^1$	[Xe]	
Pr	[Xe] $4f^3$ $6s^2$	[Xe] $4f^2$	[Xe] $4f^1$	
Nd	[Xe] $4f^4$ $6s^2$	[Xe] $4f^3$	[Xe] $4f^2$	[Xe] $4f^4$
Pm	[Xe] $4f^5$ $6s^2$	[Xe] $4f^4$		
Sm	[Xe] $4f^6$ $6s^2$	[Xe] $4f^5$		[Xe] $4f^6$
Eu	[Xe] $4f^7$ $6s^2$	[Xe] $4f^6$		[Xe] $4f^7$
Gd	[Xe] $4f^7$ $5d^1$ $6s^2$	[Xe] $4f^7$		
Tb	[Xe] $4f^9$ $6s^2$	[Xe] $4f^8$	[Xe] $4f^7$	
Dy	[Xe] $4f^{10}$ $6s^2$	[Xe] $4f^9$	[Xe] $4f^8$	[Xe]$4f^{10}$
Ho	[Xe] $4f^{11}s^2$	[Xe] $4f^{10}$		
Er	[Xe] $4f^{12}$ $6s^2$	[Xe] $4f^{11}$		
Tm	[Xe] $4f^{13}$ $6s^2$	[Xe] $4f^{12}$		[Xe] $4f^{13}$
Yb	[Xe] $4f^{14}$ $6s^2$	[Xe] $4f^{13}$		[Xe] $4f^{14}$
Lu	[Xe] $4f^{14}$ $5d^1$ $6s^2$	[Xe] $4f^{14}$		
Y	[Kr] d^1 $5s^{2.}$	[Kr]		

1.2.3.3 The atomic and ionic radius of lanthanides

Lanthanide contraction

Lanthanide contraction refers to the gradual decrease in atomic and ionic radii observed across the lanthanide series, from lanthanum (La) to lutetium (Lu), as the atomic number increases. This size reduction arises primarily due to the progressive increase in nuclear charge across the series. However, unlike in typical periods where added electrons occupy outer shells, in the lanthanides the additional electrons are placed in the inner 4f subshell [25].

The 4f electrons are relatively poor at shielding the increased nuclear charge due to their diffuse spatial distribution and limited penetration. Consequently, the outer electrons in the 5s and 5p orbitals experience a progressively stronger effective nuclear charge. This enhanced electrostatic attraction between the nucleus and the outer electrons leads to a contraction in both atomic and ionic sizes despite the increasing number of electrons. The incomplete shielding by the 4f electrons is therefore a key factor responsible for this phenomenon [28].

Lanthanide contraction leads to several noticeable effects;

One effect of lanthanide contraction is the similarity with Yttrium (Y^{3+}). The radius of the Y^{3+} ion is between that of Ho^{3+} and Er^{3+} and the atomic radius of yttrium lies between neodymium and samarium. Because of this, yttrium shows chemical properties similar to those of the lanthanides. In some systems, it may behave more like the lighter lanthanides, and in others, more like the heavier ones, depending on how covalent the bonding is [31].

The radius of lanthanide ions decreases gradually as the atomic number increases, resulting in regular changes in the properties of lanthanide elements as the atomic number increases. For example, the stability constant of lanthanide complexes usually increases, the alkalinity of lanthanide ions decreases and the pH at which hydrates start to precipitate from an aqueous solution decreases gradually as the atomic number increases[29, 31].

The contraction is more noticeable in lanthanide ions than in neutral atoms. This is because the shielding effect of 4f electrons is weaker in atoms than in ions. (**Figure 1. 12**) shows how the ionic radius changes across lanthanide series [31].

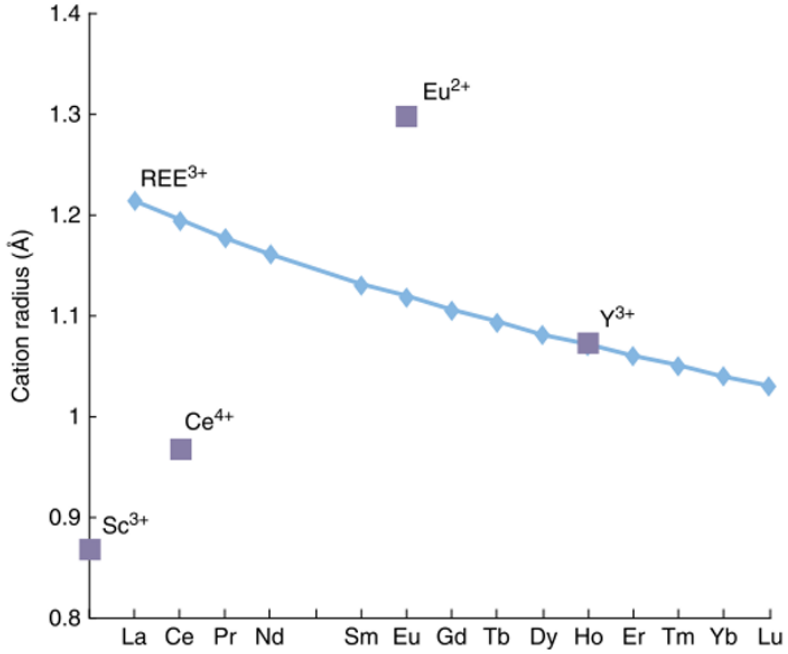

Figure 1. 12 The decreasing trend of the lanthanide ions across the period.

The atomic radii decrease across the series but the trend is not regular, three elements Cerium (Ce), europium (Eu), and ytterbium (Yb) show exceptions to this trend. This is due to differences in their metallic electron configurations.

Europium (Eu) and ytterbium (Yb) prefer stable half-filled ($4f^7$) and fully filled ($4f^{14}$) configurations, respectively, and typically contribute only two conduction electrons. This reduced electron cloud overlap results in a larger atomic radius than other lanthanides [19].

Cerium, on the other hand, can contribute more conduction electrons, which increases the overlap between atoms and makes its atomic radius smaller than expected [26, 32].

1.2.3.4 The luminescence properties of lanthanides

Luminescence refers to the emission of light by a substance that has absorbed energy but not due to heat hence it is often called "cold light." It arises from spontaneous radiative transitions where electrons in a material drop from higher-energy states to lower-energy ones, including the ground state. These emissions occur without the thermal agitation associated with incandescence.

Luminescence encompasses several subtypes depending on the energy source triggering the emission, such as photoluminescence (from light), electroluminescence (from electric current), chemiluminescence (from chemical reactions), and others [20].

1.2.3.4.1 Lanthanide based luminescence

Lanthanide ions (Ln^{3+}), especially those in the trivalent state, exhibit unique luminescence features due to their shielded 4f electrons, which give rise to sharp emission lines. Their f–f emission lines cover the entire spectrum, from ultraviolet (Gd^{3+}), visible (Pr^{3+}, Sm^{3+}, Eu^{3+}, Tb^{3+}, Dy^{3+}, Ho^{3+}, Er^{3+}, Tm^{3+}) and infra-red (Pr^{3+}, Nd^{3+}, Sm^{3+}, Dy^{3+}, Ho^{3+}, Er^{3+}, Tm^{3+}, Yb^{3+}). These transitions are Laporte-forbidden, meaning they are symmetry-restricted and typically weak in absorption with absorption coefficient ε (0.1 to 10 L. $mol^{-1}.cm^{-1}$). However, luminescence can be significantly enhanced by coordination with suitable organic ligands through a mechanism known as the Antenna effect [33, 34].

1.2.3.4.2 Mechanism of the antenna effect (ligand to metal energy transfer*)*

The organic ligand absorbs ultraviolet or visible light, promoting an electron to an excited singlet state. The excited electron may undergo non-radiative decay to a lower-energy triplet state. The energy is then transferred from the ligand's triplet state to an excited state of the lanthanide ion. The lanthanide ion returns to the ground state through characteristic f–f transitions, emitting light (fluorescence or phosphorescence) as illustrated in (**Figure 1. 13**). This pathway allows the efficient sensitization of lanthanide ions by light-absorbing ligands such as β-diketonate, phenanthroline derivatives, crown ethers, and other chromophoric systems.[28, 35].

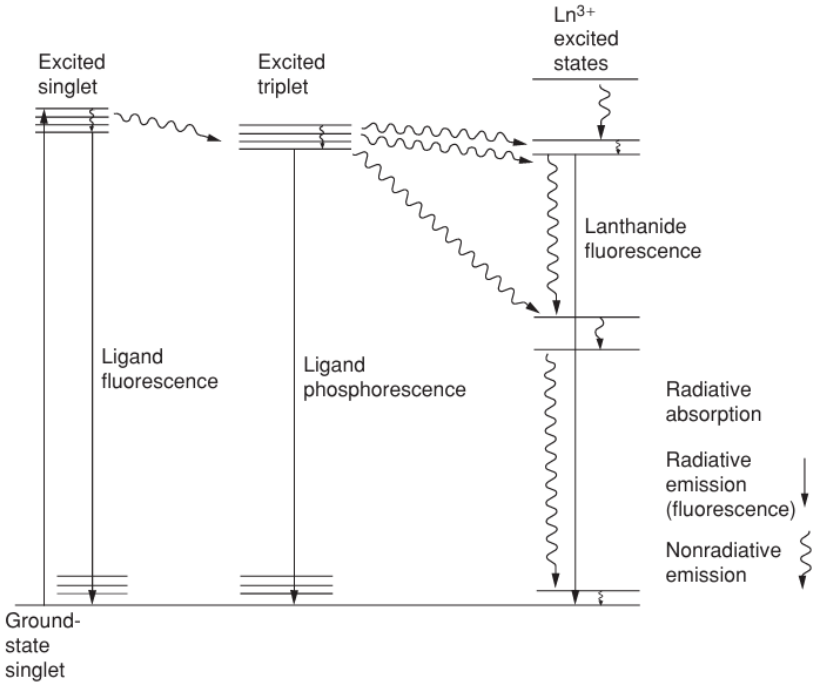

Figure 1. 13 Luminescence in lanthanide complexes[28].

1.2.4 Application of lanthanide complexes

Lanthanides are renowned for their magnetic, catalytic, and structural versatility**:** Several lanthanides (for example Gd^{3+}, Dy^{3+}) exhibit paramagnetic or ferromagnetic behaviour, which is used in MRI (Magnetic Resonance Imaging) contrast agents and permanent magnets [36].

Catalytic Applications; Lanthanide ions act as hard Lewis's acids, easily coordinating with ligands and polarizing bonds, making them excellent catalysts in organic transformations**.** Widely employed in petroleum refining (for example fluid catalytic cracking using lanthanide-doped zeolites). Cerium-based oxides are key components in automobile catalytic converters, facilitating the oxidation of toxic exhaust gases (CO, NO_x, hydrocarbons) into benign byproducts (CO_2, H_2O) [37].

Other Industrial Uses; lanthanides are essential in the manufacture of specialty glasses and lasers due to their optical properties. They are also used in high-strength alloys, particularly in aerospace and electronics applications [38].

Bioimaging and molecular probes; Eu^{3+} and Tb^{3+} complexes are widely used in biological imaging due to their long luminescence lifetimes, narrow emission bands, and resistance to photobleaching. These complexes allow time-resolved fluorescence, reducing background noise in biological samples [39].

Chapter 1: Coordination chemistry and rare earth metals

Organic light-emitting diodes (OLEDs) and displays; lanthanide complexes serve as highly efficient red and green emitters, especially in OLED technologies. Their sharp emission bands result in vivid and stable colour outputs in display panels[40]

Security inks and anti-counterfeiting; lanthanide-based phosphors are used in banknotes, ID cards, and official documents to prevent counterfeiting. They glow under UV light, making hidden marks or patterns that are not visible in normal light. Because their glow is strong and lasts a long time, they are ideal for creating secure, tamper-proof labels [6].

Medical diagnostics; time-resolved luminescence using lanthanide chelates enables sensitive assays with reduced background autofluorescence, enhancing diagnostic accuracy. Widely applied in fluorescence immunoassays**,** DNA detection**,** and in vivo imaging [41].

Environmental and chemical sensors; lanthanide luminescence can be modulated in response to metal ions, pH levels, or oxygen concentration, making them effective as chemical and environmental sensors [42].

Chapter 2: Materials and Methods

Chapter 2 : Materials and Methods

In this chapter, we present the different synthesis methods used in the development of our compounds. We also describe the different characterization methods and techniques used to identify and study their properties.

2.1 Synthesis Methods of coordination compound

2.1.1 Diffusion Reaction

High nuclearity complexes are often insoluble in various solvents once they are formed, which prevent further recrystallization. Thus, to obtain a single-crystal structure, with adequate size and quality must be directly formed from the synthesises. Slow Diffusion technique in a glass tube is an important method for the preparation of coordination compounds and the growth of crystals [12].

This method is carried out at room temperature in fine tubes of about 0.3cm diameter containing two different miscible reactant solutions with different densities, separated by 1ml pure solvent (one of the solvents used). The separated solutions will begin to diffuse into and through the intervening solvent to form desired crystals. The crystal begins to form after some weeks or months [43].

The inconvenience of this method is that it's very slow and takes long to form the crystals, there is too much difficulty in retrieving the crystals from the tube, also the yield quality is very small.

2.1.2 Hydro/solvothermal synthesis

The term hydrothermal is purely of geological origin. It was first used by the British geologist Sir Roderick Murchison (1792–1871) to describe the action of water at elevated temperature and pressure, in bringing about changes in the earth's crust leading to the formation of various rocks and minerals.

Byrappa and Yoshimura (2001) define hydrothermal as any homogeneous or heterogeneous chemical reaction in the presence of a solvent (whether aqueous or non-aqueous) above the room temperature and at pressure greater than 1 atmosphere in a closed system. However, there is still some confusion with regard to the very usage of the term hydrothermal. For example, chemists prefer to use a term solvothermal, meaning any chemical reaction in the presence of a non-aqueous solvent or solvent in supercritical or near supercritical conditions[44].

Chapter 2 : Materials and Methods

Hydrothermal and solvothermal techniques are ideal for producing crystalline, thermally stable complexes that may not form under ambient conditions by turning parameters; (temperature, pressure, solvent).

The reaction percussors (metal, ligands, solvents) are transferred into the teflon lined stainless steel autoclave shown in **(Figure 2. 1)** of which the filling percentage does not exceed 80% of its volume. The vessel is well closed to withstand the high pressure (autogenerated from heating of about 120 to 200°C for several hours). The high pressure build up is due to solvent vaporization enhancing solubility and reactivity thus the crystal growth is favored [12].

Figure 2. 1 Teflon lined stainless steel autoclave.

Table 2. 1 Factors influencing hydro/solvothermal synthesis.

Parameter	**Effect**
Temperature	Higher temperature increase solubility but may decompose sensitive ligands
Reaction time	Longer durations improve crystallinity but may also cause formation of side products
Ph	Affects ligand coordination mode and metal hydrolysis
Concentration	Higher concentrations may lead to faster nucleation but smaller crystals
Fill volume	Typically, 60 to 80% of the autoclave capacity to maintain the pressure

2.2 Methods of characterisation

2.2.1 Diffraction of X rays on powders

X-rays are high energy electromagnetic waves with wavelengths in the order of interatomic distances (~0.1–0.2 nm).

X-ray diffraction (XRD) is a versatile, non-destructive analytical method used to analyse material properties like phase composition, structure, texture and many more of powder samples, solid samples or even liquid ones. Identification of phases is achieved by comparing the X-ray diffraction pattern obtained from an unknown sample with patterns of a reference database [45].

In powder XRD, the sample (which is finely ground and homogeneous) comprises an immense number of microcrystalline domains (crystallites) randomly oriented in space. Due to this random orientation, the diffracted X-rays from all possible crystal planes are detected when the angle between the incident beam and detector is systematically varied. This provides a complete pattern of intensities versus angles (2θ), which reflects the sample's structural fingerprint [46].

The output of an XRD experiment is a diffractogram: a plot of X-ray intensity versus 2θ. The positions (angles) of the peaks correspond to specific interplanar spacings (d-values), while the intensity is related to the atomic arrangement and crystallographic texture. The observed pattern is compared to reference databases such as the ICDD (International Centre for Diffraction Data) PDF database**.** (PDF-4+ or COD (Crystallography Open Database)**.**

Crystallite size can be estimated using the Scherrer equation:

$D=K\lambda /\beta\cos$

- D is the average crystallite size,
- K is the shape factor (usually ~0.9),
- λ is the X-ray wavelength,
- β is the full width at half maximum (FWHM) of the peak in radians,
- θ is the Bragg angle.

Lattice parameters are calculated based on peak positions (using Bragg's Law) illustrated in (**Figure 2. 2**) $n\lambda=2d\sin\theta$ [46].

where:

- n is the order of reflection,
- λ is the wavelength of incident X-rays,
- d is the distance between atomic planes,
- θ is the angle of incidence

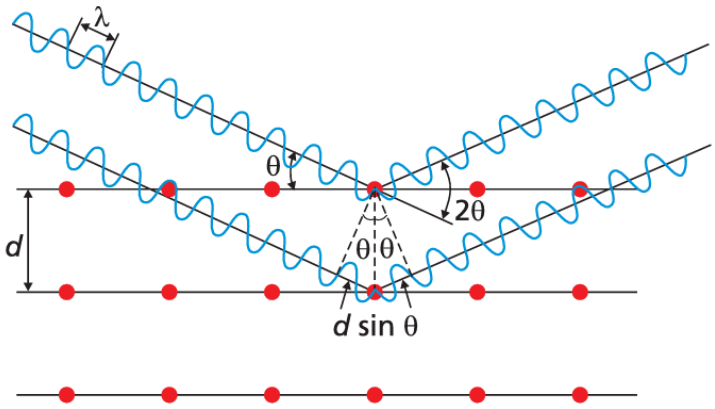

Figure 2. 2 Illustration of Bragg's Law showing incident and reflected X-rays on parallel crystal planes [46].

During this study, all the powder diffractograms were registered with in the range of 5-50 °(2θ) with the help of Rigaku Mini-Flex II (LPCMC) diffractometer (**Figure 2. 3**), by using radiations of Cu-ka (λ=1.5406 Å) with a scan step of 0.03° (2θ).

This analysis helped us to verify the originality of our compounds and also to confirm the compounds in the same family before proceeding to single crystal DRX analysis.

Figure 2. 3 Rigaku Mini-Flex II (LPCMC) diffractometer.

2.2.2 Infra-red Spectroscopy

Infrared (IR) spectroscopy is a widely used technique for identifying functional groups and studying molecular vibrations. It involves the interaction of infrared radiation (wavelength range: 0.7 to 500 µm or wavenumber range: 14,300 to 20 cm^{-1}) with matter. Within this region of the electromagnetic spectrum, chemical compounds absorb IR radiation when there is a dipole moment change during a normal molecular rotation/vibration (bending or stretching).

An IR spectrometer consists of three basic components:

- Radiation source (emits infra-Red radiations)
- monochromator (separates infra-red radiations into different wave lengths)
- and detector (measures the absorbed or transmitted IR spectrum [47, 48].

IR absorption information is generally presented in the form of a spectrum with wavelength or wavenumber (cm^{-1}) as the x-axis and absorption intensity or percent Transmittance, T, as the y axis. The IR spectrum is made up of three major regions; near IR (14000 to 4000 cm^{-1}), mid IR (4000 to 400$cm^{-1)}$ and the far IR (400 to 10 cm^{-1}) Peaks are assigned to specific bond vibrations based on their position and intensity [49].

IR spectroscopy is used in; identification of functional groups, confirmation of ligand coordination e.g., shift in ν(C=O), ν(N–H) monitoring complex formation, hydrogen bonding, symmetry changes analysis of metal-ligand interactions in coordination complexes (especially in the far-IR region) [50].

In this study, all the IR spectra were registered at room temperature with the help of the PerkinElmer Spectrum 2FT-IR ATR (LPCMC) spectrometer (**Figure 2. 4**) with in (4000-400 cm^{-1}), with the ATR (Attained Total Reflectance) method and a resolution of 4 cm^{-1}.

This analysis helped us to confirm the presence and fixation of ligands on the central metals.

Figure 2. 4 The Perkin Elmer Spectrum 2FT-IR ATR (LPCMC) spectrometer.

2.2.3 Thermogravimetric analysis (TGA)

Thermogravimetric analysis (TGA) is a thermal analysis technique used to measure changes in the mass of a sample as it is heated over time. This method is particularly useful in studying material stability, decomposition patterns, and compositional analysis. TGA monitors the mass of a sample (ranging from 1 mg to several grams) as it is heated up to 1600°C in a controlled atmosphere (inert e.g. N_2, oxidative, or vacuum) [51].

A thermogravimetric analyser consists of a high precision balance (measures the mass of the sample), the furnace (for heating), the thermocouple (for accurate temperature reading), gas control system (air for oxidation) and the crucible (holds the sample).

The results of this analysis are given in form of a thermogram which illustrates different phases of decomposition of a sample by the present mass in relation to temperature. The changes in mass are as a result of decomposition, dehydration, sublimation and oxidation. [44, 52].

The thermograms presented in this in this work are registered by the help of the Labsys Evo gas option TG DSC 1600°C (SETARAM)(LPCMC) thermic analyser (**Figure 2. 5)**.

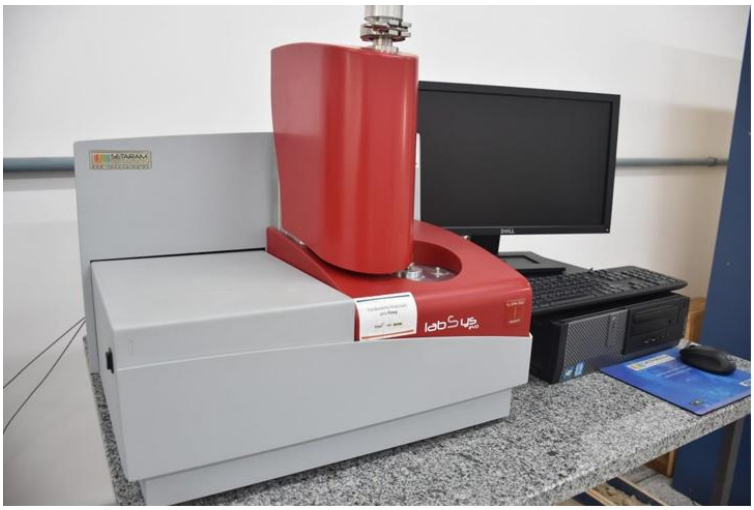

Figure 2. 5 Labsys Evo gas option TG DSC 1600°C (SETARAM)(LPCMC) thermic analyser.

2.2.4 Optic microscopy

Optical microscopy also known as light microscopy is a technique that uses visible light and a system of lenses to magnify small samples, allowing for the visualization of microstructural features that are not discernible to the naked eye.

The basic components of an optical microscope include an objective lens, an ocular lens (eyepiece), and a light source. The technique relies on the interaction of light with the sample surface. Light is transmitted or reflected through the sample, and lenses are used to focus and magnify the image, which can be observed directly or captured digitally.

The resolving power of an optical microscope is governed by the wavelength of light used and the numerical aperture (NA) of the objective lens. Typically, the resolution limit is around 200 nm, which allows observation of microstructural features such as grain boundaries, crystal morphology, and defects in the micrometer range [53].

Advantages

- Rapid and easy visualization of crystal morphology.
- Non-destructive and requires minimal sample preparation.
- Useful for qualitative analysis and documentation of physical appearance

Limitations

- Cannot provide information about internal crystal structure or elemental composition

- Subjective interpretation ; quantitative analysis (e.g., size distribution) requires digital image procession.

In this study, optical microscopy was employed using the optika microscopes Italy **Figure 2. 6** to observe the surface morphology, crystal shape, and size of the synthesized coordination polymers. It provided preliminary insight into the homogeneity and macroscopic characteristics of the crystals formed.

Figure 2. 6 The optika microscope.

2.2.5 Photoluminescence

Photoluminescence analysis is a spectroscopic technique used to study luminescent properties of materials in different emission ranges. It is based on emission of light by chemical species subjected to ultra violet, visible or infra-red vibration hence its name photoluminescence. It allows measurement of quantum yield and emission of lifetime of luminescent compounds and offers possibility of recording absorption and emission spectra[35].

The measurement consists of subjecting the sample to a radiation source (UV light) at a specific wave length. The absorption of this radiation by the sample results in an absorption spectrum corresponding to an electronic transition from ground state to excited state. The absorbed energy is then emitted by the sample. This response is collected by a detector, processed, and interpreted by an emission spectrum [42].

Chapter 2 : Materials and Methods

In this work, the excitation and emission spectra of luminescent compounds were recorded using a Shimadzu RF-6000 spectrophotometer (LPCMC) (**Figure 2. 7)**. Measurements were collected at room temperature in the UV-visible range (450 to 800 nm), using solid-state samples.

Figure 2. 7 Shimadzu RF-6000 spectrophotometer.

2.3 . Materials used

2.3.1 The ligands

2.3.1.1 Pimelic acid

Pimelic acid or heptanedioic acid is an aliphatic dicarboxylic acid, with a molecular formular $HO_2C(CH_2)_5CO_2H$, molecular mass of 160.167 $g.mol^{-1}$. It is a white crystalline solid insoluble in water.

Due to its two terminal carboxylic acid groups, pimelic acid functions as a bidentate or bridging ligand, capable of coordinating two metal centers through the deprotonated carboxylate groups ($–COO^-$). This makes it particularly valuable in constructing polymeric metal complexes or coordination polymers**,** where extended network structures are formed [54].

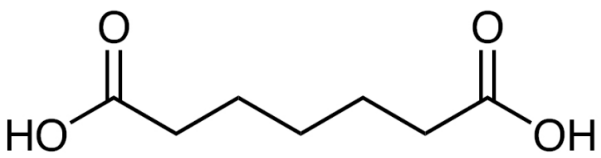

Figure 2. 8 Structure of pimelic acid.

2.3.1.2 Isophthalic acid

Isophthalic acid is an organic compound with the formular $C_6H_4(CO_2H)_2$, preferred IUPAC name benzene-1,3-dicarboxylic acid, other name meta-phthalic acid. It is a white crystalline solid insoluble in water with molar mass of 166.132gmol-1. The 1,3-substitution pattern allows for extended angular or zigzag bridging between metal centers making it suitable for constructing multidimensional frameworks.

The delocalised π electrons in the benzene structure provide a rigid backbone that resists rotation and conformation changes which helps in building crystalline structures with defined porosity [55].

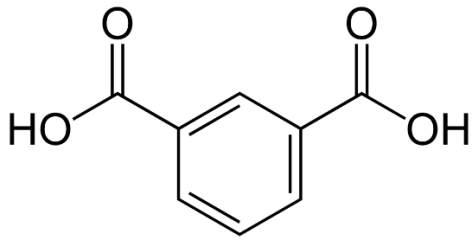

Figure 2. 9 structure isophthalic acid.

2.3.2 Lanthanide metals

The choice of lanthanide metals was done in consideration of the variation of the atomic radius across the group in the periodic table; that is to say, we considered those at the start of the group, (La), the middle (Gd) and the far end (Yb) of the group in each set of series of manipulation. The metals used include Lanthanum (La), Gadolinium (Gd), Praseodymium (Pr), Neodymium (Nd), Samarium (Sm), Terbium (Tb), Dysprosium (Dy), Erbium (Er), and Ytterbium (Yb).

Chapter 3: Results and discussion

Chapter 3 : Results and Discussion

In this chapter, we present the synthesis, structural characterization, and discussion of various series of coordination polymers based on lanthanide (Ln^{3+}) ions using pimelic acid and isophthalic acid as organic ligands. These compounds were synthesized and characterized through established experimental techniques, and the obtained results are compared with reported structures in the literature.

3.1 Literature review: lanthanide coordination polymers with pimelic and isophthalic acids.

Previous research has widely explored the use of pimelic acid and isophthalic acid individually with lanthanide metals. However, the combination of both ligands in the same coordination framework remains largely unexplored, presenting a novel area for investigation. The literature reveals a variety of structural motifs depending on the ligand, coordination mode, and metal ion.

Below in (**Table 3. 1**) is a summary of some known coordination polymers involving the use of these two ligands separately with pimelic acid having only two different structures and isophthalic acid having seven different structures:

Table 3. 1 Examples of some of coordination polymers formed with pimelic and isophthalic acid and lanthanide metals.

Chemical formular	**Metals**	**References**
Isophthalic acid structures (ip denotes Isophthalate)		
$[Ln_2(ip)_3(H_2O)_2]_n$	La, Gd, Nd, Sm, Eu, Tb	[56],[57][58][59], [60]
$[Ln_2(ip)_2(Hip)_2(H_2O).H_2O]_n$	La, Nd, Sm, Tb	[61][60], [62]
$[Ln_2(ip)_2(hip)_2(H_2O)]_n \cdot nH_2O$	La, Pr, Nd	[63],[64]
$[Ln_2(H_2O)_2(ip)_3] \cdot H_2O$	Gd, Dy, Y	[64][65][66]
$[Ln_2(OH)(ip)_2(Hip)(H_2O)_8 \cdot 6H_2O]$	Ln, Sm, Dy	[67]
$[K_2Eu_2(ip)_4(H_2O)_4.8H_2O]$	Eu	[68]
$[Tb(ip)(Hip)(H_2O)_4.3H_2O]$	Tb	[68]
Structures with pimelic (pim=pimelate)		
$[Ln(pim)(Hpim)(H_2O)].H_2O$	Pr, Ce, La	[69], [70]
$[Ln_2(pim)_3(H_2O)_4]$	Er, Tb	[69]

Chapter 3 : Results and Discussion

The simulated patterns were generated using Mercury software from CIF files of structurally resolved compounds. The simulated X-ray diffraction patterns of coordination polymers available in the literature were obtained by simulation using Mercury software from their CIF files obtained through structural resolution.

From this literature overview, it is evident that the individual application of isophthalic acid and pimelic acid leads to the formation of a rich diversity of coordination polymer structures. The differences in rigidity (isophthalic acid being rigid and aromatic, and pimelic acid being flexible and aliphatic) allow each ligand to play a distinct structural role. Therefore, the simultaneous use of both ligands introduces the possibility of synergistic effects, potentially yielding new structural motifs and photophysical properties not accessible with either ligand alone.

3.2 Synthesis of coordination polymers

The coordination polymers in this study were synthesized by two methods; hydrothermal synthesis and synthesis by slow diffusion in fine tubes. Both techniques were employed to optimize crystal quality and structural diversity. Further details on the synthetic conditions for each complex are presented in the following sections.

3.2.1 Synthesis by hydrothermal method

Uunder this method, several experimental parameters were varied, including the molar ratios of lanthanide ions to the two ligands (isophthalic acid and pimelic acid), reaction temperature, and the heating duration in the oven. Throughout all experiments, the pH was carefully maintained at 4.5.

Experimental Conditions

Seven distinct sets of synthesis conditions were employed, as summarized in (**Table 3. 2**) below.

Table 3. 2 The hydrothermal synthesis conditions that were used for coordination polymer formation

Ratio (Ln^{3+}/isophthalic/pimelic)	**Temperature(°C)**	**Time(hrs)**
1/1/1.5	170	48
1/1/1.5	150	66
1/2/2	150	108
1/2/2	170	66
1/2/2	150	72

1/1.5/1	150	96
1/1.5/1	170	66

For each condition, five replicates were prepared following the same procedure with 5 different Ln^{3+}.

Synthesis Procedure

- **Preparation of the mixture**

A total of 100 mg of the lanthanide salt ($LnCl_3 \cdot 6H_2O$ or $Ln(NO_3)_3 \cdot 6H_2O$, where Ln = (La, Nd, Sm, Tb, Dy, Er or Yb) was dissolved in a mixture of 5 mL bidistilled water and 5 mL methanol. The appropriate stoichiometric amount of isophthalic acid (as per the molar ratio) was added to this solution and stirred for 30 minutes at room temperature using a magnetic stirrer. The required mass of pimelic acid was then introduced, and the mixture was stirred for an additional 30 minutes under the same conditions.

- **pH Adjustment**:

The pH of the solution was adjusted to 4.5 by the dropwise addition of some drops of 1 M NaOH solution.

- **Thermal Treatment:**

The resulting solution was transferred into a 25 mL Teflon-lined stainless-steel autoclave, which was sealed and heated at the specified temperature (150 °C or 170 °C) for the appropriate duration (as listed in Table 2.4). After heating, the autoclave was allowed to cool at a rate of 10 °C/hr to room temperature (25 °C).

- **Post-Reaction Workup.**

Upon cooling, a white precipitate was observed in all reactions.

1. First Filtration:

The precipitate was separated from the reaction mixture by filtration. The solid (residue) was washed with bidistilled water and left to dry at room temperature for slow evaporation. The filtrate, a clear solution, was retained for further filtration.

2. Second Filtration:

The filtrate was kept at room temperature to allow for slow evaporation. Over time, white grain-like crystalline powders formed, which were collected by a second filtration. Both the newly formed solid and the filtrate were again left at room temperature for continued evaporation. This process was repeated until the filtrate fully evaporated.

As a result, seven different series of coordination polymers were obtained and labelled as Series 1 to Series 7.

3.2.2 Synthesis by slow diffusion

In this method, the crystallization of coordination polymers was achieved through slow diffusion under varying experimental conditions. These conditions included adjustments in the molar ratios of the reactants, the choice of solvents, and the spatial arrangement of the reaction components within the diffusion setup. Two molar ratios of lanthanide ion to isophthalic acid to pimelic acid were investigated; 1/1/1.5 and 1/2/2. The lanthanide sources employed were either lanthanide (III) chloride hexahydrate $[LnCl_3].6H_2O$ or lanthanide (III) nitrate hexahydrate $[Ln(NO_3)_3].6H_2O$ where Ln = Dy, Gd, Yb, La, or Pr.

Three solvents were used in this synthesis that is methanol (MeOH), tetrahydrofuran (THF) and bidistilled water. Each reaction mixture consisted of:

- 10 mg of the lanthanide salt
- Stoichiometric masses of isophthalic acid and pimelic acid according to the chosen molar ratio
- 1 mL methanol
- 1 mL bidistilled water
- 1 mL THF

Experimental Setup

The slow diffusion technique was carried out using vertically arranged glass tubes. The placement and arrangement of reactants followed three distinct configurations, illustrated in

(**Figure 3. 1).** These configurations aimed to explore how spatial setup influences diffusion behaviour and crystal formation.

For each of the three configurations, a total of ten diffusion tubes were prepared, five using methanol and five using THF. A few drops of distilled water were carefully added between the solvent layers to aid in the gradual interdiffusion of the phases thereby supporting controlled crystal growth. This was applied to the two molar ratios. All the tubes were covered properly to prevent evaporation of the solvents.

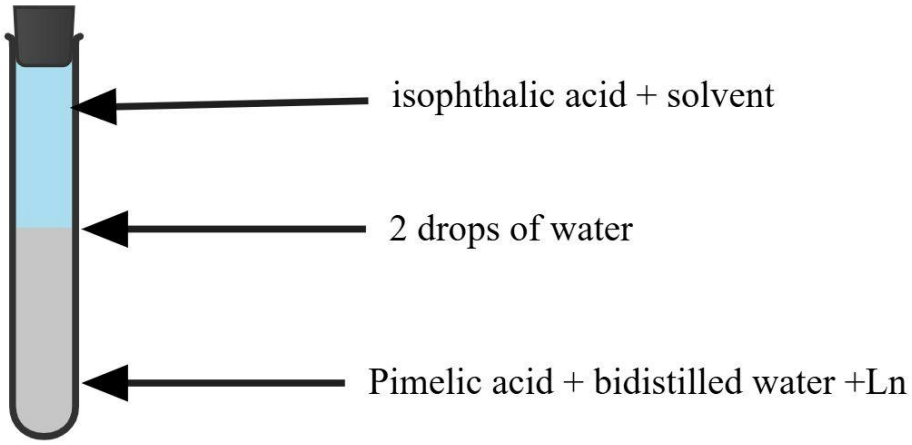

Figure 3. 1 first configuration arrangement of the reactants.

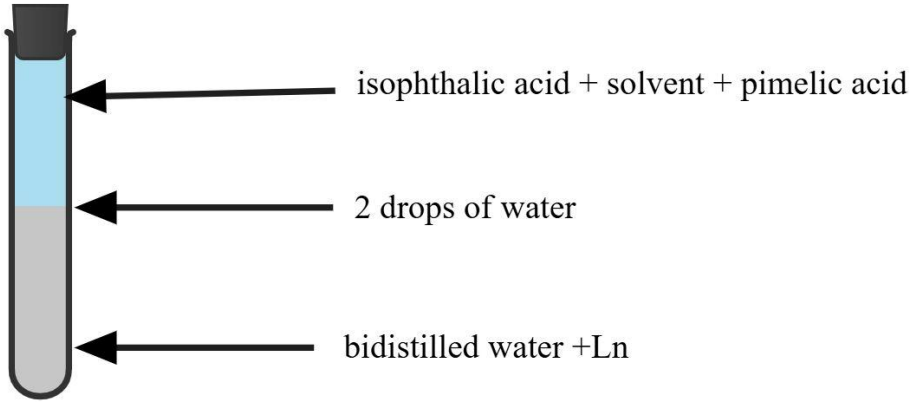

Figure 3. 2 second placement configuration.

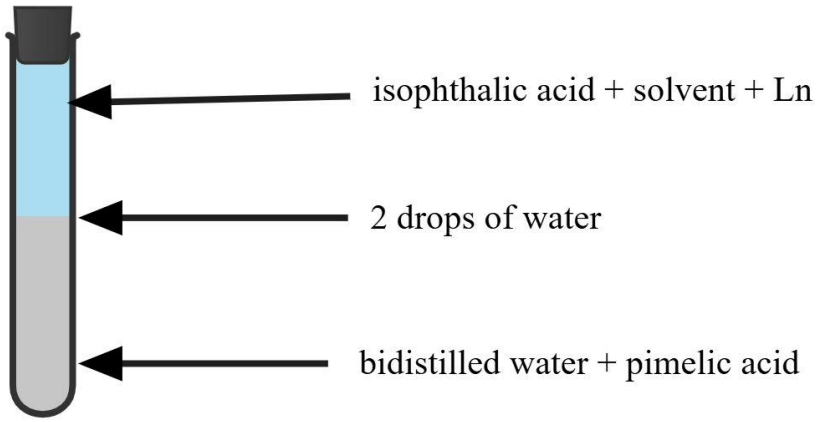

Figure 3. 3 third placement configurations.

Figure 3. 4 shows some of the tubes prepared during slow diffusion synthesis method.

Figure 3. 4 Photograph showing selected tubes prepared for the slow diffusion experiments.

Crystal nucleation and growth were not synchronous across all tubes. The onset and rate of crystal formation varied, with some tubes exhibiting crystal development earlier than others. This variability is likely attributed to subtle differences in diffusion rates, temperature fluctuations, and solubility dynamics within the individual setups. Below is a photograph (**Figure 3. 5**) of one of the tubes containing the formed crystals.

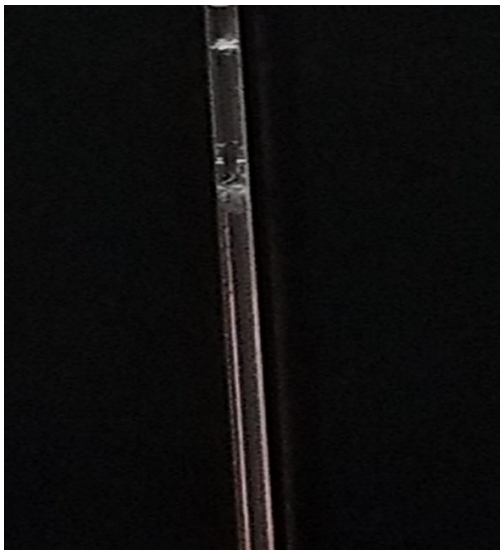

Figure 3. 5 tube containing crystals.

3.3 Discussion of the results

3.3.1 Characterization of the ligands

Before analysing the coordination polymers, it is essential to first characterize the individual ligands used in the synthesis, pimelic acid and isophthalic acid in order to identify their characteristic functional group vibrations. This allows for a better understanding of ligand coordination behaviour in the resulting complexes.

In this case we carried out infra-red spectroscopy analysis and powder X ray diffraction on the two acids.

(**Figure 3. 6**) presents the infrared (IR) spectrum of pimelic acid showing its main absorption bands. The corresponding assignments of vibrational modes are summarized in **(Table 3. 3)**, which highlights the functional groups present and serves as a reference for later comparison with the spectra of the synthesized coordination polymers. Also, the PXRD pattern of pimelic acid is represented in (**Figure 3. 7**).

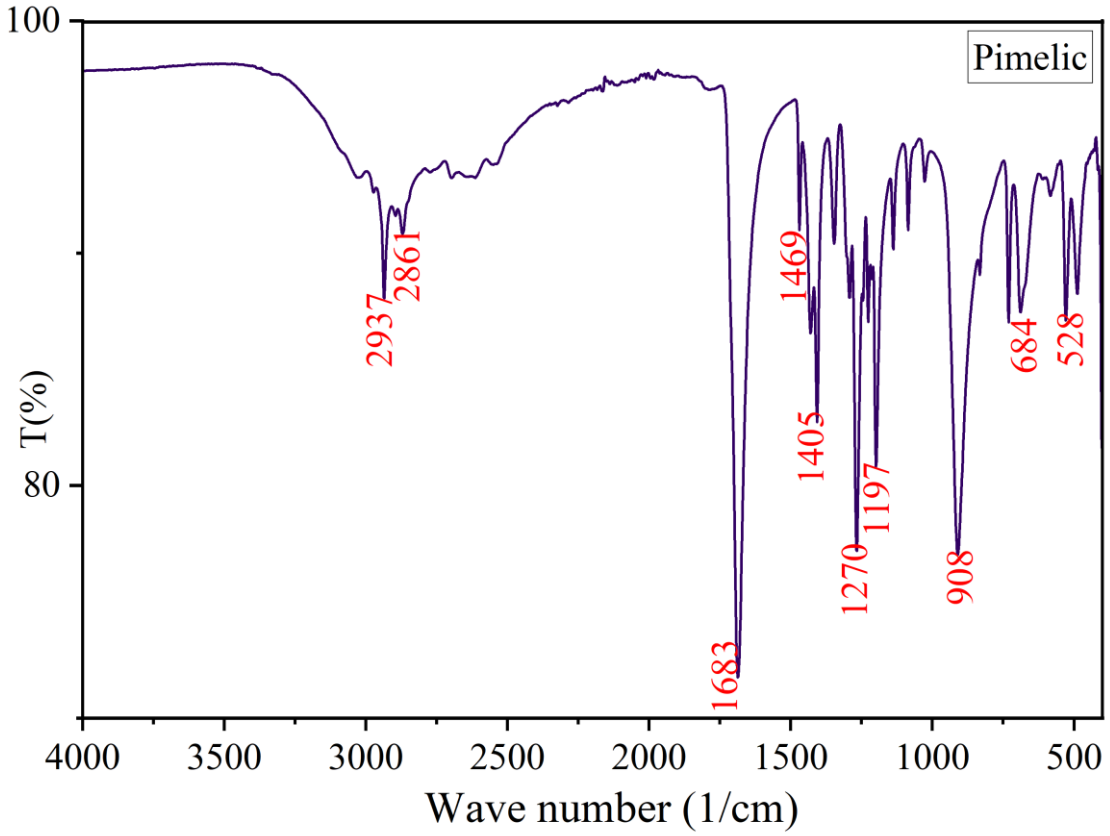

Figure 3. 6 Infra-Red spectrum of pimelic acid

Table 3. 3 The vibration bands of pimelic acid [63][64].

Wave number(cm^{-1})	**Intensity**	**Functional group**	**Type of vibration**	**Explanation**
2500–3010	Broad	ν(O-H) (carboxylic acid)	Stretching	band due to hydrogen bonding between COOH groups
2861 to 2937	Weak	ν(C-H) CH_2 (alkyl)	Stretching	The C–H bonds in the (CH_2) groups
1683	Strong	ν(C=O) (carboxylic acid)	Stretching	Carbonyl group stretch
1469	Weak	(δ)CH_2	Bending	In-plane bending of the methylene C–H bonds.

1405	Medium	δ(O-H)	Bending	In-plane bending vibration of hydroxyl group
1270	Medium	ν(C–O)	Stretching	Stretching of the C–O bond in COOH
908	Weak	δ (O-H)	Bending	out-of-plane bending (called O–H deformation)
750 to 685	Weak	γ(CH_2)	rocking	Rocking motion of methylene (CH_2) groups in long carbon chains.

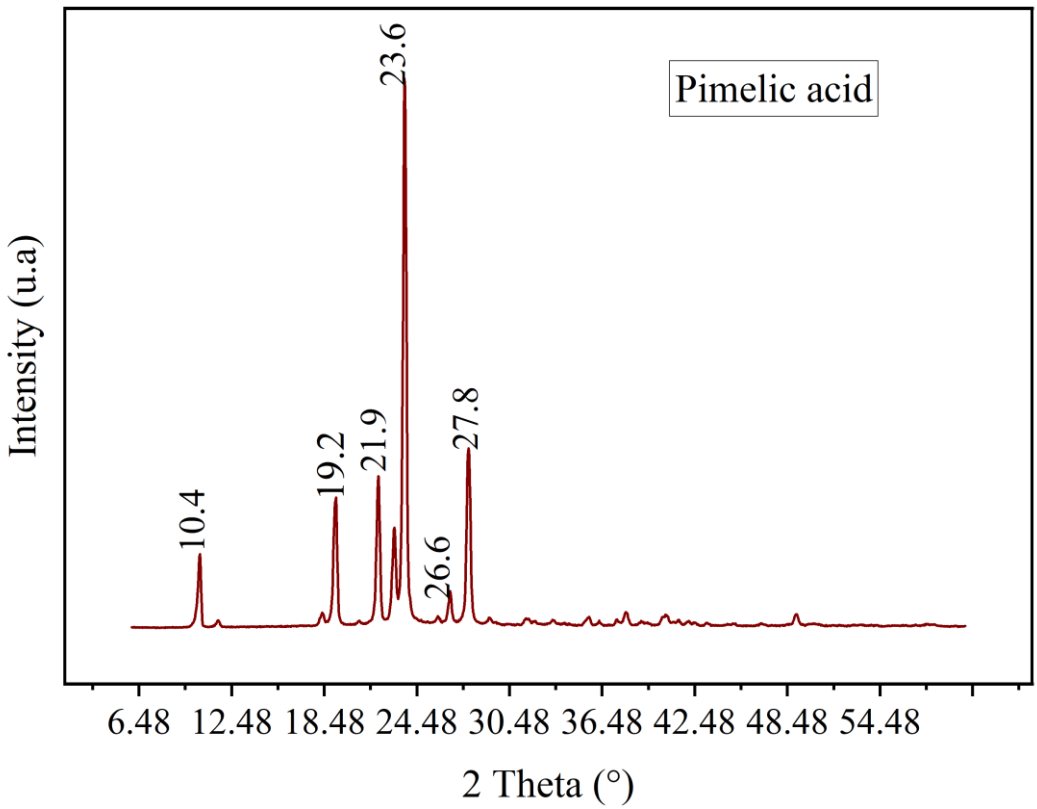

Figure 3. 7 Powder X ray diffraction pattern of pimelic.

The infra-red spectrum of isophthalic acid is represented in (**Figure 3. 8**) showing the important absorption bands.

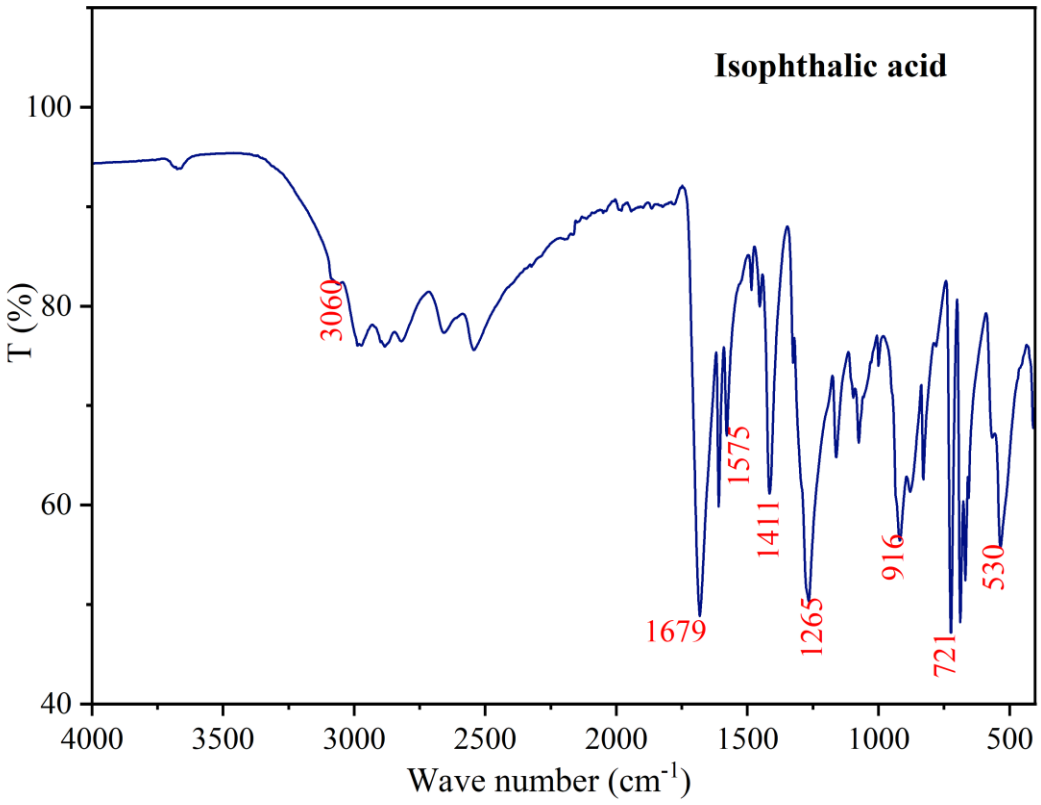

Figure 3. 8 Infra-red spectrum of isophthalic acid.

The corresponding assignments of vibrational modes are summarized in (**Table 3. 4**) which highlights the functional groups present and serves as a reference for later comparison with the spectra of the synthesized coordination polymers.

Table 3. 4 vibration bands of isophthalic acid [41, 65].

Wave number(cm^{-1})	**Intensity**	**Functional group**	**Type of vibration**	**Explanation**
2500–3100	Broad, strong	ν(OH) (carboxy)	Stretching	broad stretch due to hydrogen bonding in COOH
3060	Weak	ν(C-H)	Stretching	C–H stretching vibration of aromatic hydrogen atoms.
1680	Strong	ν(C=O)	Stretching	Sharp band due to Carbonyl group stretch

1450–1600	Medium to weak	ν(C=C)	Stretching	C=C stretching modes in the benzene ring.
1415	Medium,	δ(O–H)	Bending	O–H in-plane bending from the –COOH group.
1260	strong	ν(C–O)	Stretching	Associated with the COOH group
912	medium	δ(O–H)	bending	Out of plane O–H deformation
700	strong	δ(C-H)	Bending	Indicative of meta substitution pattern on benzene ring

Also, the PXRD pattern of isophthalic acid is represented in (**Figure 3. 9**).

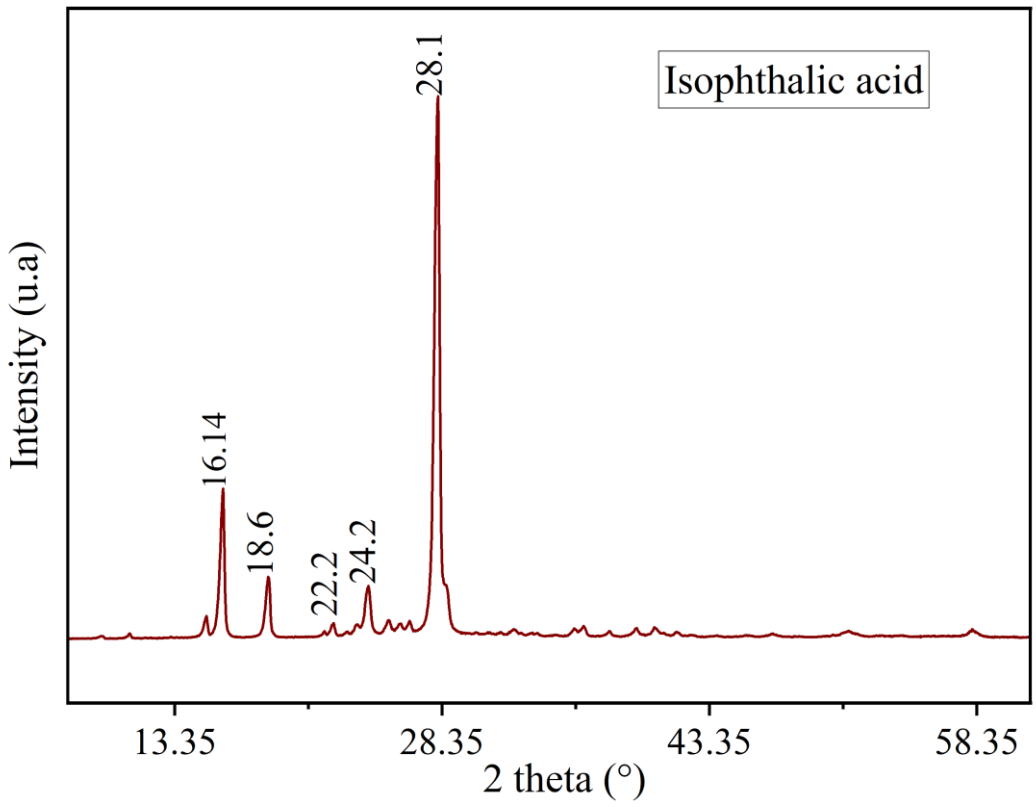

Figure 3. 9 PXRD diffractogram of isophthalic acid.

3.3.2 Characterization of the compounds obtained from slow diffusion

Following the synthesis of the coordination polymers by slow diffusion process, various characterization techniques were employed to analyse their physical and structural properties. These included, optical microscopy and infrared (IR) spectroscopy.

3.3.2.1 Optical microscopy

The crystals collected were mounted on clean glass slides and covered with coverslips. No staining or additional preparation was necessary, as the crystals were clearly visible under ambient light conditions. The optical images revealed that the coordination polymer crystals exhibited needle-like, block-like, and irregular morphologies, suggesting varied crystal growth habits depending on synthesis conditions. Below in (**Table 3. 5**) are some of the shapes of the of the representative examples of these crystals.

Table 3. 5 different morphology of the crystals obtained from slow diffusion.

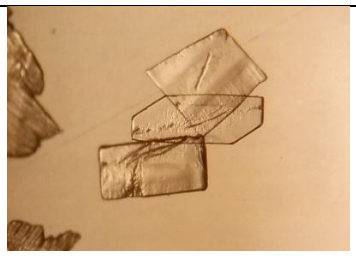	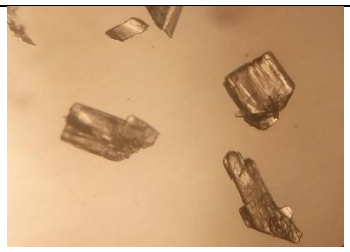	
block like shaped crystals (well defined rectangular prisms).	irregular shaped rough crystals	The long needle like crystals.

Considering the observed morphologies, the block-like crystals, due to their well-defined geometry and suitability for diffraction studies, were selected for single-crystal X-ray diffraction (SCXRD) analysis. However, we were not able to perform the SCXRD at this time due to a lack of access to the necessary equipment. We are currently exploring options to collaborate with other laboratories that have the required facilities, and we hope to carry out the analysis when the opportunity becomes available.

To protect the selected crystals and maintain their quality, no further tests were done on them. Instead, we repeated the same slow diffusion method to grow more of these crystals. These new samples are still in the laboratory, as crystallisation is a long process.

The remaining crystals (needle-like and irregular morphology) were then used for infra-red spectroscopy analysis.

3.3.2.2 Infrared (IR) Spectroscopy

IR spectroscopy was carried out on the irregular shaped crystals and the results were compared both among the samples and with the spectra of the free ligands, isophthalic acid and pimelic acid.

Based on the results obtained, interestingly, the IR spectra obtained closely resembled the spectrum of pure isophthalic acid as shown in (**Figure 3. 10)**, suggesting no coordination or incomplete reaction involving the ligands under these conditions which led to the crystallization of only isophthalic acid.

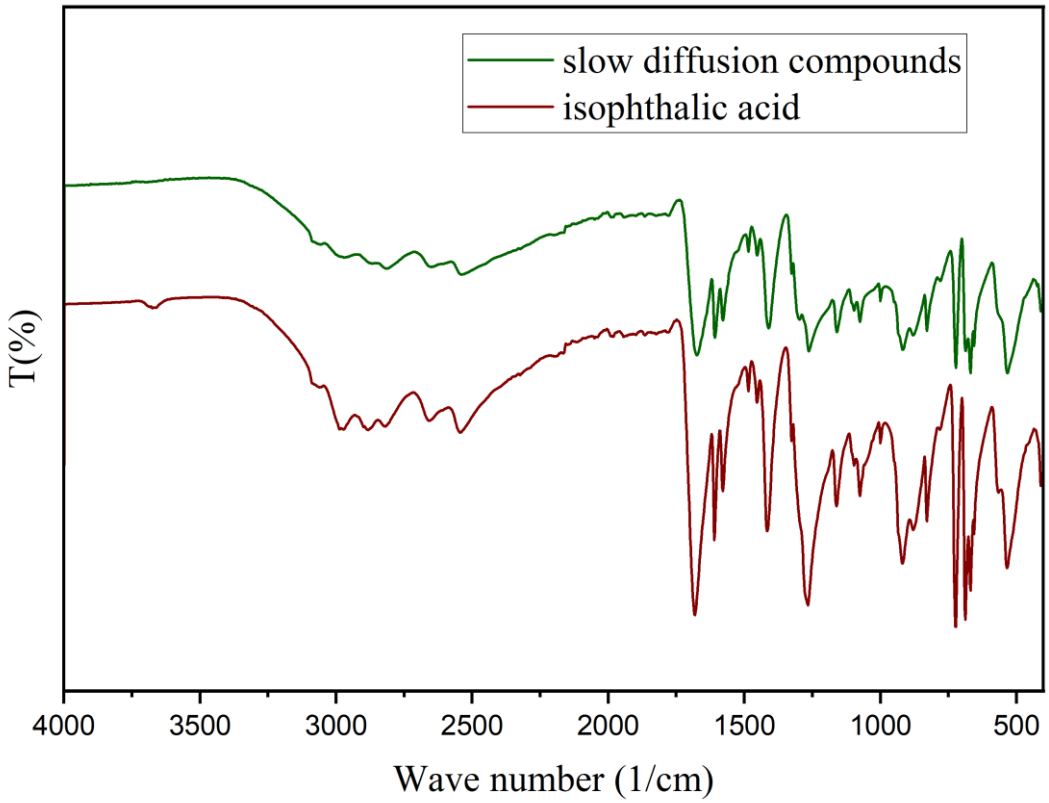

Figure 3. 10 IR spectra of isophthalic acid and the compounds obtained by slow diffusion.

3.3.3 Compounds obtained by hydrothermal synthesis

Following the synthesis of the coordination polymers through the hydrothermal method, several crystalline samples were obtained. To examine their chemical composition and

structural similarities properties, a combination of infra-red spectroscopy and powder Xray diffraction were employed.

- **Infra-red spectroscopy**

Infra-red spectroscopy analysis was performed on all compounds obtained by hydrothermal synthesis method. Their spectra were compared amongst the samples and then with the infra-red spectra of the ligands. The results showed that all the hydrothermally synthesized compounds had IR spectra that were clearly different from those of the free acids. However, they still displayed key absorption bands associated with the ligands, suggesting that coordination had taken place and that the metal ions were incorporated into the ligands.

- **Powder X-ray Diffraction (PXRD)**

PXRD was a key tool used for the selection and differentiation of the synthesized compounds. The diffraction patterns of all the obtained samples were recorded, and seven distinct series of coordination polymers were identified from the hydrothermal synthesis based on differences in their PXRD patterns. These were selected for further analysis.

Subsequently, the PXRD patterns of the selected compounds were compared with simulated PXRD data from known lanthanide coordination polymers reported in the literature.

Confirmation of structural novelty/ originality

From the PXRD comparison with literature;

Three of the seven selected compounds showed PXRD patterns that did not match any known structures, indicating they are novel coordination polymers; that is from series 1 to series 4.

The other three compounds (series 5 to 7) showed patterns matching previously reported structures but with different lanthanide ions, indicating that they are isostructural analogs of known compounds.

3.3.3.1 Serie 1

The series comprises four compounds incorporating different lanthanide metal ions: lanthanum (La), neodymium (Nd), samarium (Sm), and terbium (Tb) obtained through the first filtration in hydrothermal synthesis method.

3.3.3.1.1 Infra-Red Spectroscopy

The IR spectra of all four compounds show highly similar patterns, as illustrated in (**Figure 3. 11)**, indicating similarity in their chemical composition across the series. It completely confirms the presence of the two ligands (Isophthalate and pimelate).

A broad absorption band observed at 3307 cm^{-1} is attributed to the O–H stretching vibrations, suggesting the presence of water molecules and the weak band at 2954 cm^{-1} corresponds to the ν(C-H) vibration stretching of the CH_2 in pimelate.

Significant bands at 1594 cm^{-1} and 1508 cm^{-1} are assigned to the asymmetric stretching vibrations (ν_{as}) of coordinated carboxylate (COO^-) groups; while corresponding symmetric stretching vibrations (ν_s) appear at 1438 cm^{-1} and 1371 cm^{-1}. The observed separation between ν_{as} and ν_s values ($\Delta\bar{\upsilon} \approx 156\ cm^{-1}$ and $137\ cm^{-1}$) suggests that the carboxylate groups adopt a bidentate/bridging coordination mode with the lanthanide ions. [71].

Additional absorption band at 1162.79 cm^{-1} is ascribed to C–O stretching of the COOH. A band at 736 cm^{-1} corresponds to the out-of-plane bending of aromatic C–H groups which confirms the presence of Isophthalate.

A weak band at 657 cm^{-1}corresponds to the γ(CH_2) rocking motion of methylene (–CH_2–) groups in pimelate.

In the far-infrared region at 433 cm^{-1} is a weak band assigned to (Ln–O) stretching vibrations indicating successful coordination of the ligands to the metal center through oxygen donor atoms[72].

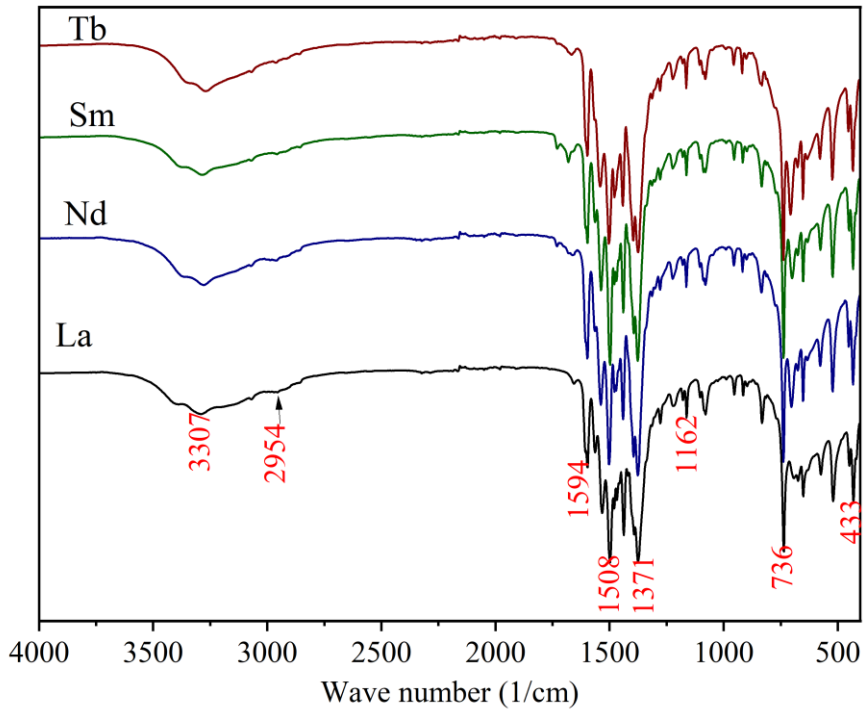

Figure 3. 11 infra-red spectrum of series 1.

3.3.3.1.2 Powder X ray Diffraction on series 1

Powder X-ray diffraction analysis was conducted to investigate the crystallinity and phase purity of the series. As shown in **(Figure 3. 12)**, the PXRD patterns of the La, Nd, Sm, and Tb complexes in this series exhibit nearly identical diffractograms, indicating that all four compounds share a similar structural framework.

Each pattern displays multiple, sharp, well-defined peaks in the 2θ range of 5° to 50°, indicating a highly crystalline nature of the synthesized compounds. The homogeneity of peak profiles across the series further supports the high purity of the synthesized materials.

While the La, Nd, Sm, and Tb complexes show a similar peak distribution, there are minor noticeable shifts in peak positions and intensities. This reflects expected structural tuning arising from metal-specific coordination preferences.[73, 74].

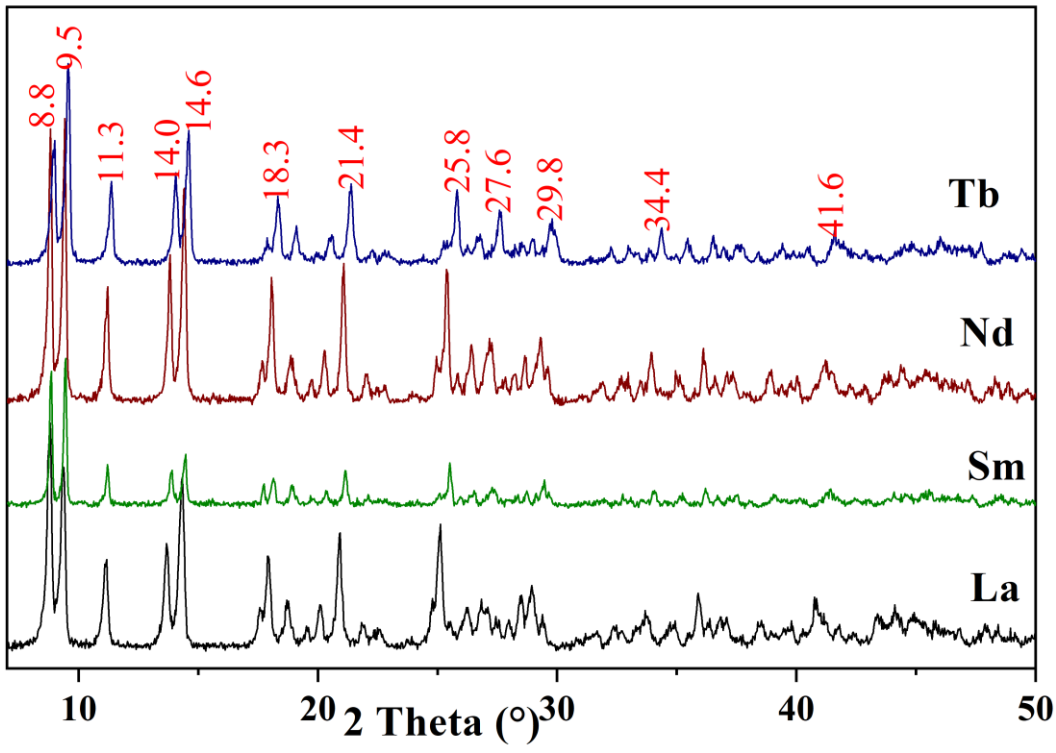

Figure 3. 12 diffractogram of series 1.

3.3.3.1.3 Thermal analysis

The thermal stability and decomposition behaviour of the coordination compounds in Series One were investigated using Thermogravimetric Analysis (TGA) and Differential Scanning Calorimetry (DSC). Due to their isostructural nature, as confirmed by their PXRD patterns, the thermal decomposition profiles of the four compounds (La, Sm, Nd, Tb) are nearly identical. Therefore, the detailed interpretation will be provided for one representative compound.

The TGA/DSC curves for the selected compound are shown in (**Figure 3. 12)** and the interpretation in **(Table 3. *6*)**.

Table 3. 6 Interpretation of Thermogravimetric and Calorimetric Data for the Selected Compound in series 1.

Temperature range (°C)	**Weight loss (%)**	**DSC Observation**	**Assignment**
54.7 to 92.4	1.2	Endothermic peak at 62.2°C	Loss of hydration water molecules

92.4 to 250.0	7.7	Endothermic peak at 228°C	Loss of coordinated water molecules
250.0 to 400.0	Constant	None	Intermediate stability
400.0 to 468.1	10.8	Endothermic peak at 452°C	Initial decomposition of the organic ligand
468.1 to 708	28.6	Endothermic peak at 578.5	Further breakdown of the ligand

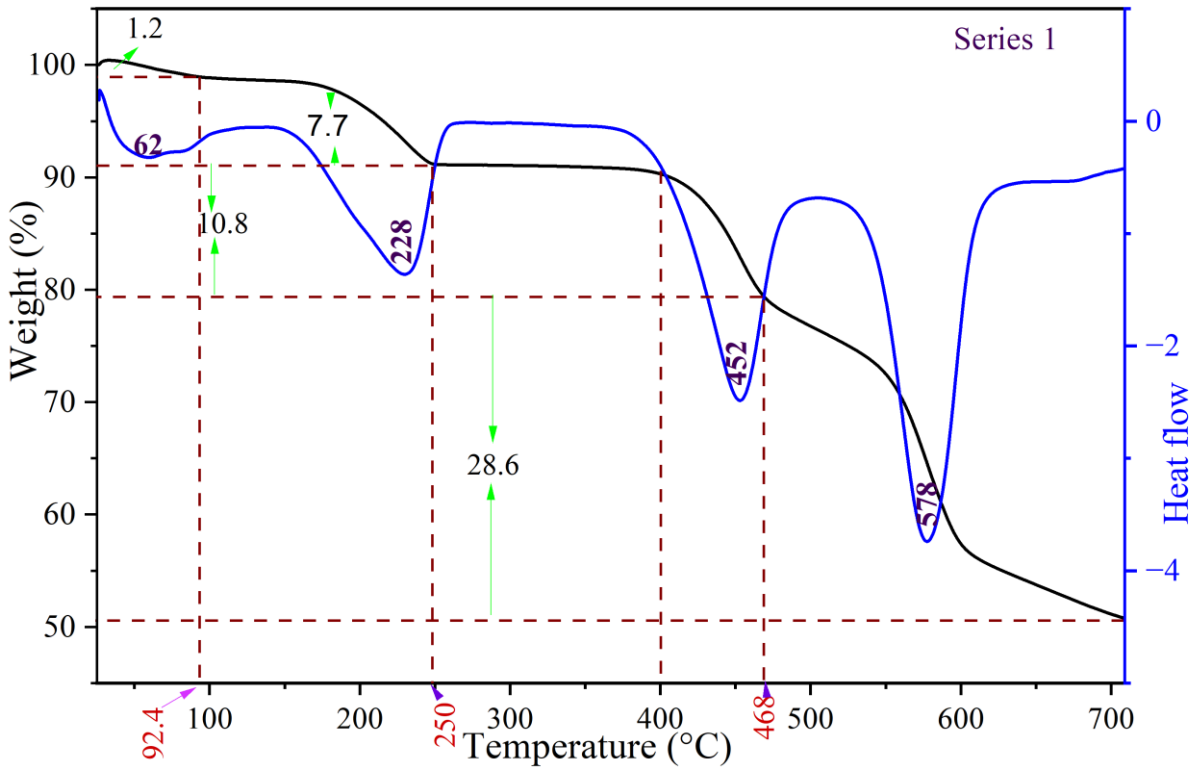

Figure 3. 13 thermogram of series 1.

3.3.3.1.4 Photoluminescence analysis

The luminescent properties of series 1 were investigated at room temperature on three solid state samples of Dy, Tb and Sm compounds. The ions Tb (III), Sm (III) and Dy (III) form complexes which exhibit ionic luminescence in the visible region.

The emission and excitation spectra of Tb complex in (**Figure 3. 14**) was recorded upon excitation wavelength of 270 nm and emission at wave length of 545 nm. The excitation spectrum displays a broad band at 270 nm attributed to the $^1\pi \rightarrow {}^1\pi^*/{}^3\pi^*$ transitions characteristic of isophthalic ligand indicating that this ligand exhibits an effective antenna effect in this compound [68].

Four emission bands are observed at 490, 545, 585 and 620 nm, are attributed to $^5D_4 \rightarrow {}^7F_6$,$^5D_4 \rightarrow {}^7F_5$, $^5D_4 \rightarrow {}^7F_4$ and $^5D_4 \rightarrow {}^7F_3$ transitions respectively. The $^5D_4 \rightarrow {}^7F_5$ band is the most dominant one. These are characteristic bands of Tb ion [37].

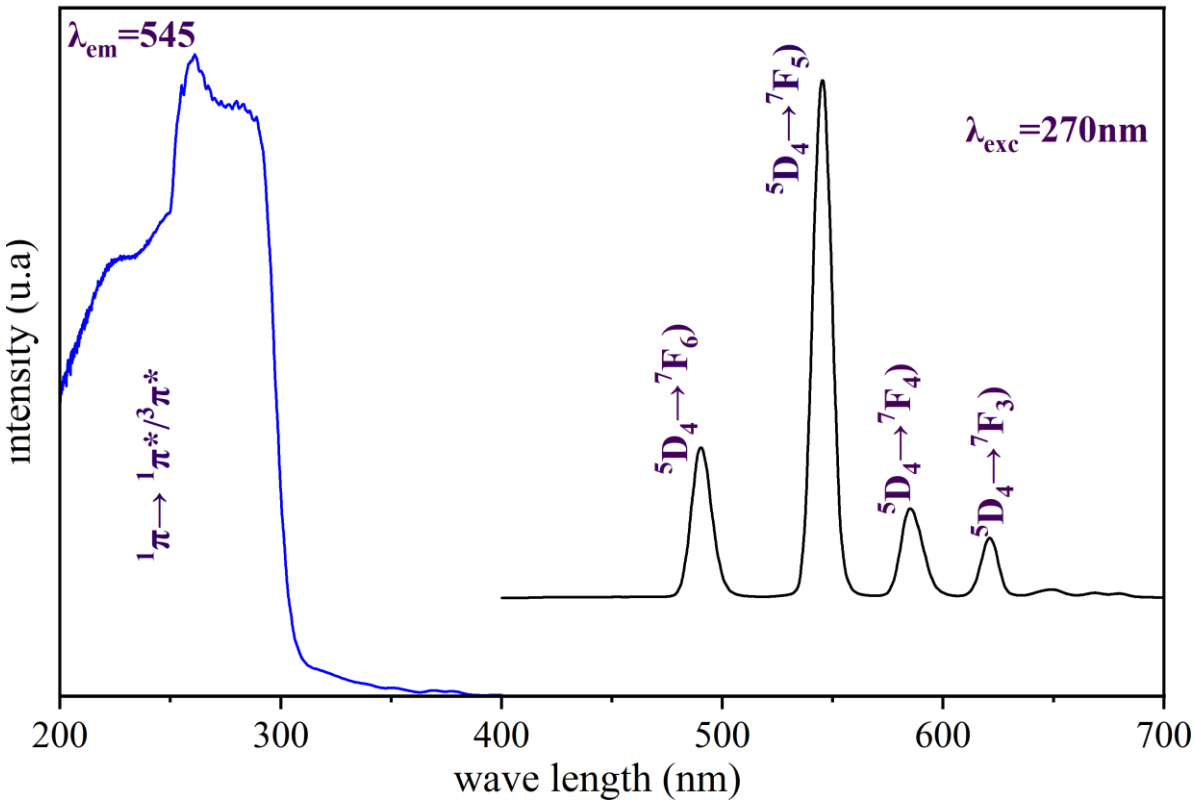

Figure 3. 14 emission and excitation spectra of Tb compound (λ_{em}=545nm, λ_{exc}=270nm).

The emission and excitation spectra of Sm complex in (**Figure 3. 15**) was recorded upon excitation wavelength of 290 nm and emission at λ_{em}=640nm. The excitation spectrum shows a broad absorption band centered at 270nm attributed to the $^1\pi \rightarrow {}^1\pi^*/{}^3\pi^*$ transition characteristic of the isophthalic acid ligand which reveals the effective antenna effect of this ligand in this compound.

Three main emission bands are observed at 560, 595 and 640 nm, which are attributed $^4G_{5/2} \rightarrow {}^6H_{5/2}$, $^4G_{5/2} \rightarrow {}^6H_{7/2}$, $_4G_{5/2} \rightarrow {}^6H_{9/2}$ transitions respectively. The $^4G_{5/2} \rightarrow {}^6F_{9/2}$ band is the most dominant one [75, 76].

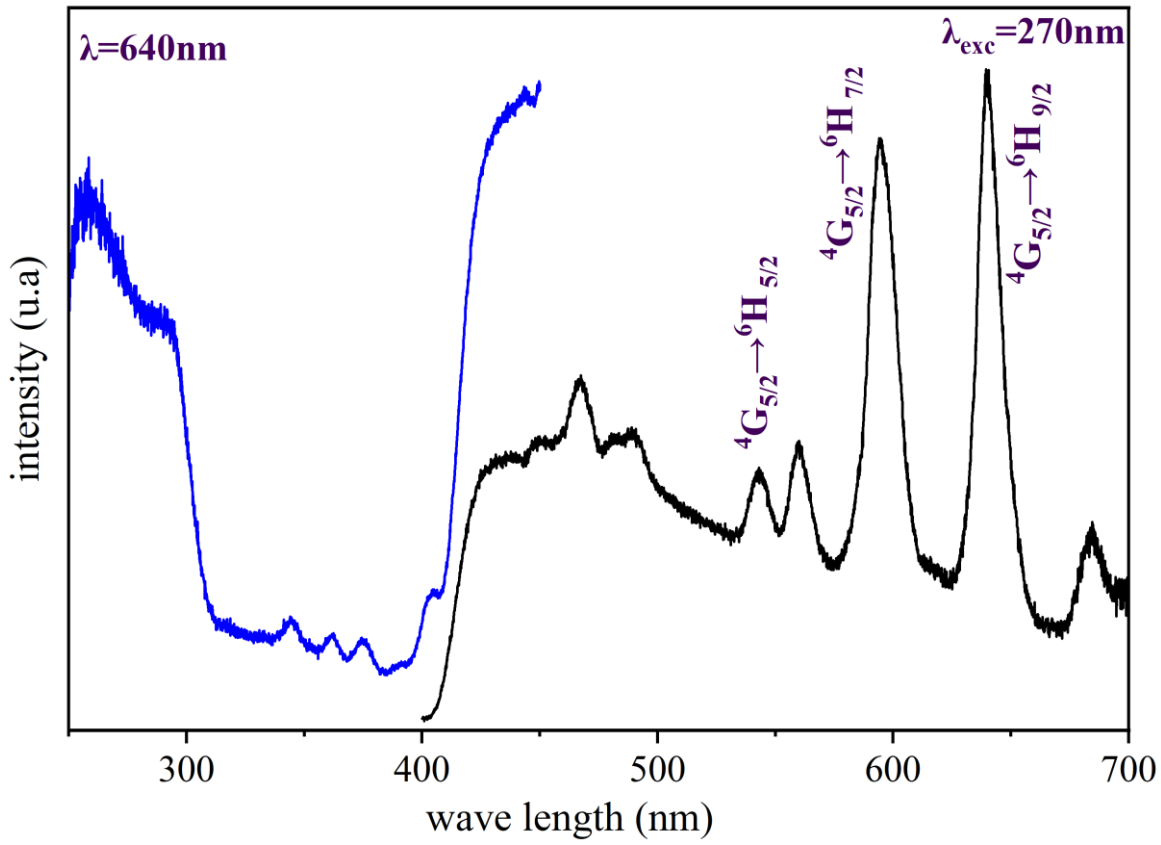

Figure 3. 15 emission and excitation spectra of Sm compound (λem=640nm, λexc=270nm).

The emission and absorption spectra of Dy in series 1 (**Figure 3. 16**) was taken at λ_{exc}=295nm and λ_{em}=545nm. The excitation spectrum displays a broad absorption band at 295 nm which is attributed to the $^1\pi \rightarrow {}^1\pi^*/{}^3\pi^*$ transitions characteristic of isophthalic ligand indicating that this ligand exhibits an effective antenna effect in this compound. In addition, there is a peak around 388 nm typical of the intrinsic $^6H_{15/2} \rightarrow {}^4F_{7/2}$ electronic transition of the Dy^{3+} ion [39].

The emission spectrum displays three prominent emission peaks at 480, 575, and 659 nm. These peaks correspond to the characteristic electronic transitions of the Dy^{3+} ion, specifically $^4F_{9/2} \rightarrow {}^6H_{15/2}$, $^4F_{9/2} \rightarrow {}^6H_{13/2}$, and $^4F_{9/2} \rightarrow {}^6H_{11/2}$, respectively. The $^4F_{9/2} \rightarrow {}^6H_{13/2}$ transition dominates the spectrum with a strong maximum peak at 575 nm, which leads to a clear mauve light emission[75].

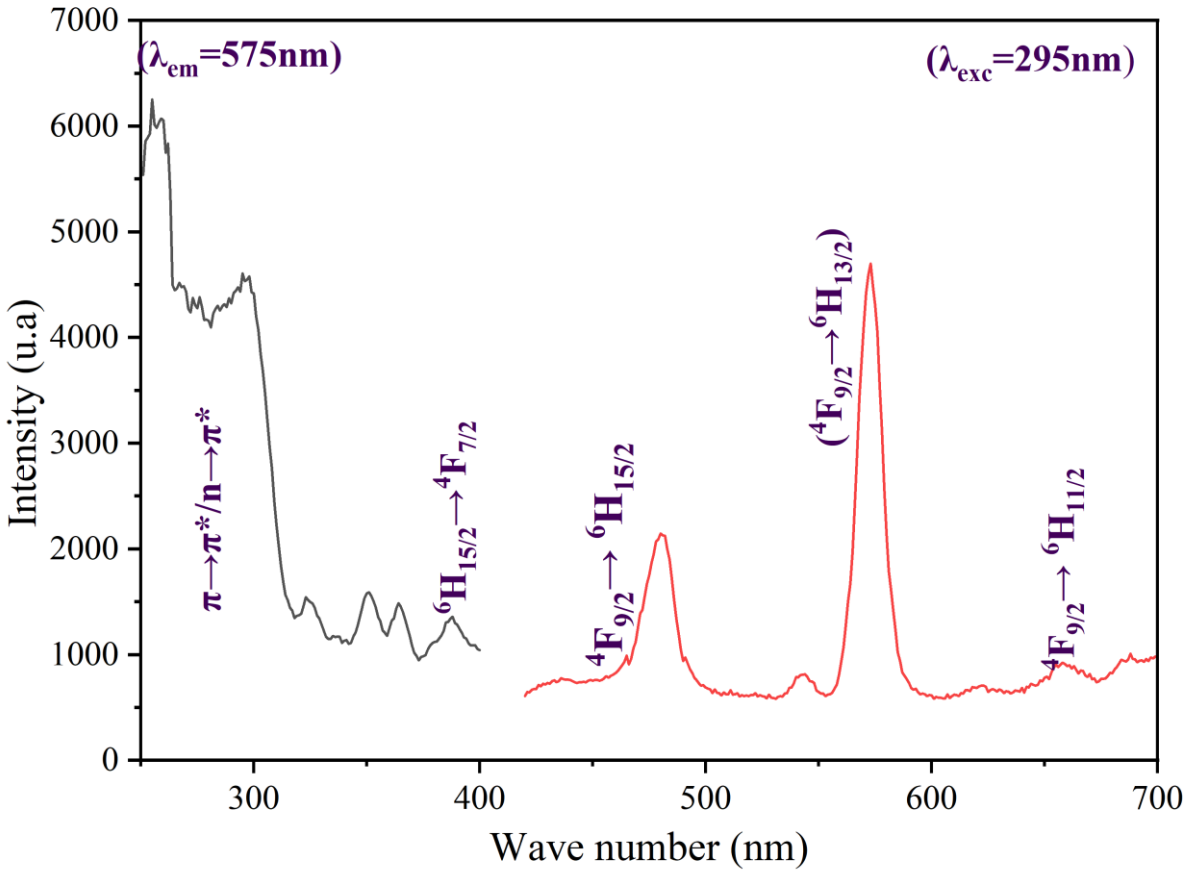

Figure 3. 16 emission and excitation spectra of Dy (λem=573nm, λexc=295nm).

3.3.3.2 Series 2

This series includes two coordination polymers synthesized using dysprosium (Dy) and terbium (Tb) as the central lanthanide ions. The compounds were synthesized under different hydrothermal conditions and all fall under the first filtration and exhibit comparable spectroscopic and structural features.

3.3.3.2.1 Infra-Red Spectroscopy

The IR spectra of both Dy and Tb complexes in Series 2 are identical and are presented in **(Figure 3. 17)**.

The band at 3278cm^{-1} is attributed to ν(O-H) vibration band of water molecules. A weak band at 2987 cm^{-1} corresponds to aliphatic ν(C-H) stretching (methylene –CH$_2$–) of pimelate. The strong bands observed at 1600 and 1521 cm^{-1} for asymmetric COO$^-$ stretching and 1450 and 1380 cm^{-1} for symmetric COO$^-$ stretch confirm complete deprotonation of both pimelic and

isophthalic acids. In this case the asymmetric (ν_{as}) and symmetric (ν_s) stretches are 150 and 141 cm^{-1} respectively, the $\Delta\bar{\upsilon}$ values in the range of 140–160 cm^{-1} typically indicates bridging coordination modes[71].

The band at 1162 cm^{-1} is ascribed to the ν (C–O) stretch in the dicarboxylate ligands, the characteristic band at 736 cm^{-1} corresponds to the out-of-plane bending of aromatic C–H groups confirm the presence of Isophthalate. A weak band at 651cm^{-1} corresponds to the γ(CH_2) rocking motion of methylene (–CH_2–) groups in pimelate. Also, a band at 1482 cm-1 represents (δ)CH_2 in-plane bending of the methylene C–H bonds. The 420 cm^{-1} band confirms (Ln–O) bond.

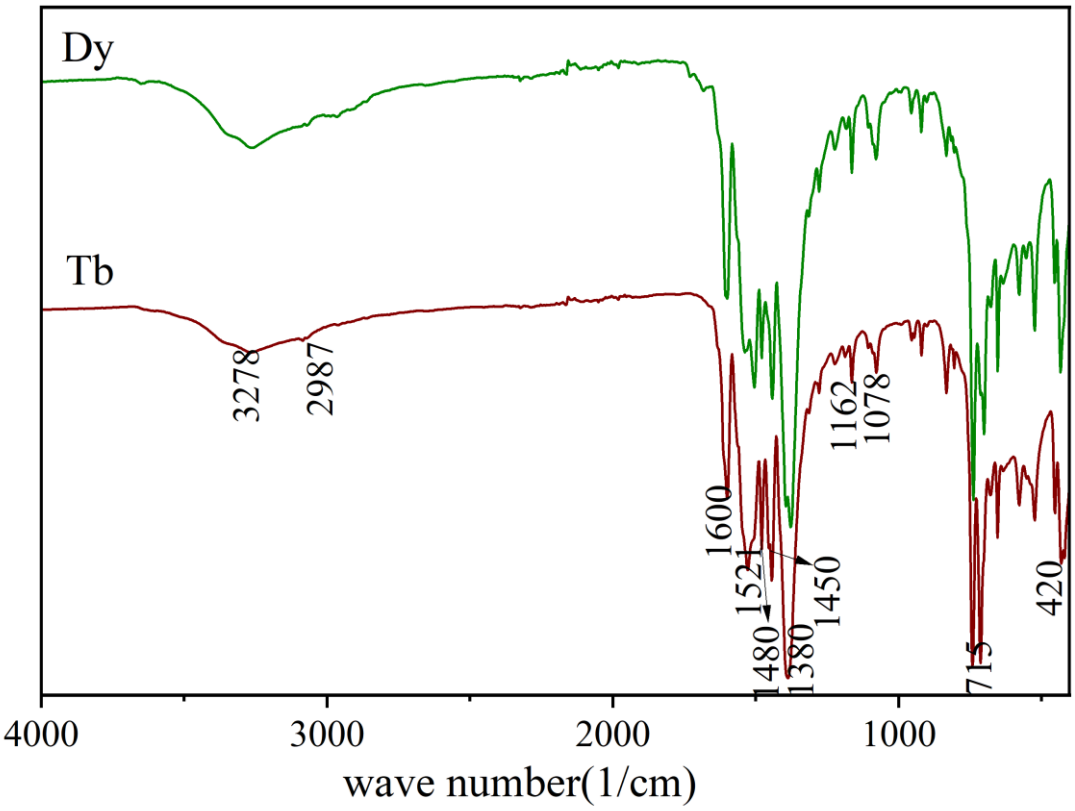

Figure 3. 17 infra-red spectrum of series 2.

3.3.3.2.2 Powder X Ray diffraction

The powder X Ray Diffraction analysis on this series gives two identical diffractograms (**Figure 3. 18**) with sharp well-defined peaks indicating pure, crystalline isostructural compounds obtained.

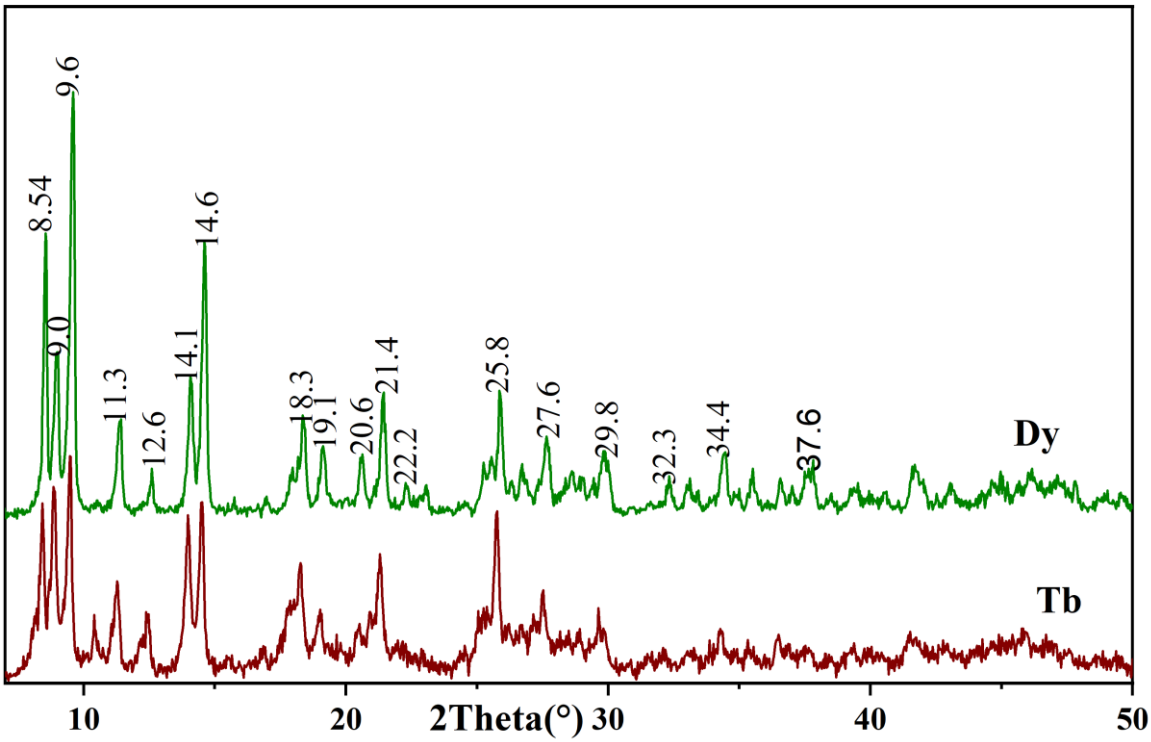

Figure 3. 18 powder Xray diffraction spectrum of series 2.

3.3.3.2.3 Thermal analysis

The thermal behaviour of the coordination compounds in Series Two was examined using Thermogravimetric Analysis (TGA) and Differential Scanning Calorimetry (DSC). The TG/DSC curves are presented in **(Figure 3. 19)**, where the black curve represents the TGA (weight loss) data, and the blue curve corresponds to the DSC (heat flow) response.

As shown in the TGA curve, the compound undergoes a multi-step decomposition process which is Interpreted in (**Table 3. 7**) below.

Table 3. 7 Thermal decomposition profile of the representative compound in series two based on TGA/DSC analysis.

Temperature Range (°C)	Weight Loss (%)	DSC Observation	Assignment
46.8 to 121.5	2.2	Endothermic peak at 54°C	Loss of water of crystallisation
121.5 to 214.1	6.7	Endothermic peak at 196°C	Loss of coordinated water molecule
214.1 to 406.5	None	None	stable intermediate
406.5 to 526.0	13.9	Endothermic peak at 498°C	Decomposition of organic ligand
525.7 to 708.7	26.7	Endothermic peak at 587°C	Further decomposition of the ligands

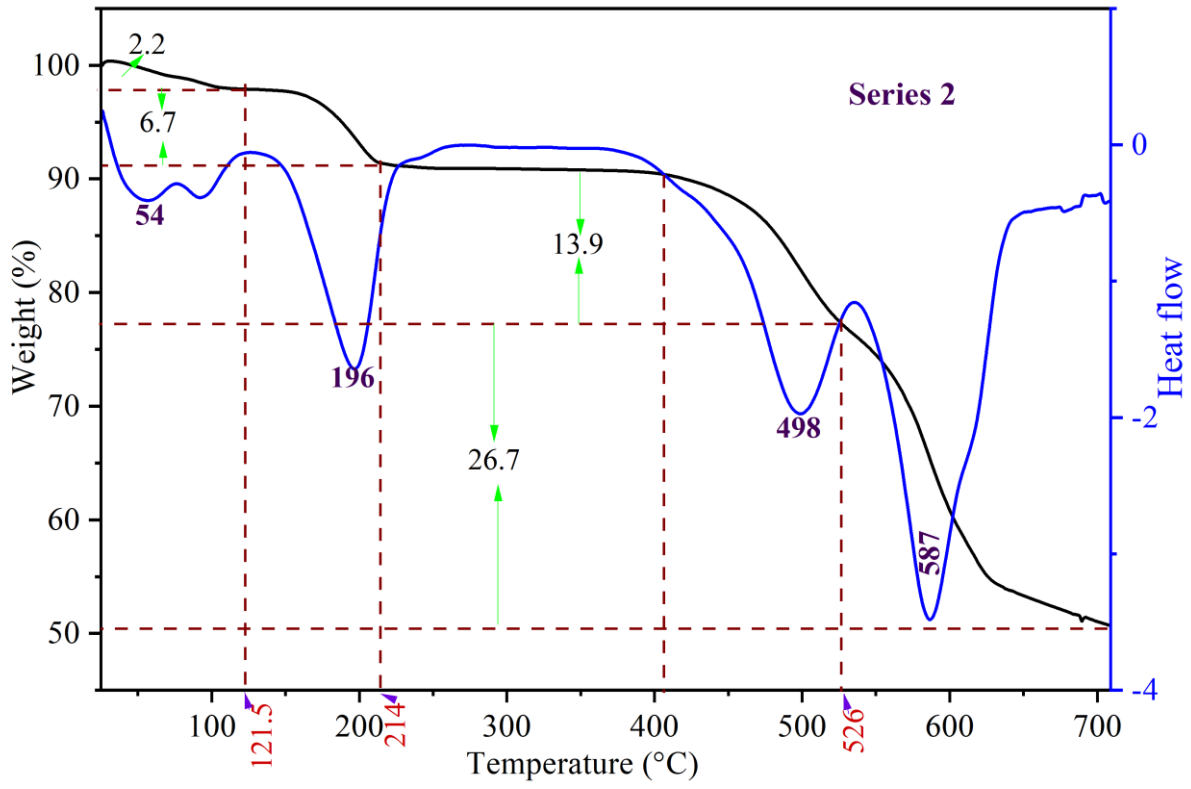

Figure 3. 19 TGA and DSC curves of the representative compound in series two showing thermal decomposition behaviour.

3.3.3.2.4 Photoluminescence analysis

The luminescent properties of series 2 were investigated at room temperature on two solid state samples of Dy, and Tb complexes at room temperature in the visible region.

The emission spectrum and excitation spectrum of Dy in series 2 registered under irradiation λ_{exc}=290 nm and λ_{em}= 575nm is shown in (**Figure 3. 20**). The excitation spectrum displays a broad band at 290 nm attributed to $^{1}\pi \rightarrow {}^{1}\pi^{*}/{}^{3}\pi^{*}$ transitions characteristic of isophthalic ligand. This confirms that the ligand effectively facilitates the antenna effect in this compound. Also, a band at 387 nm correspond to the intrinsic $^{6}H_{15/2} \rightarrow {}^{4}F_{7/2}$ electronic transition of the Dy^{3+} ion [5].

The emission spectrum shows two characteristic emission peaks of Dy (III) at 483 nm, 575 nm resulting from $^{4}F_{9/2} \rightarrow {}^{6}H_{15/2}$, from $^{4}F_{9/2} \rightarrow {}^{6}H_{13/2}$ transitions of the Dy (III) ion respectively [77]. The peak at 545 nm could be due to presence of a terbium impurity.

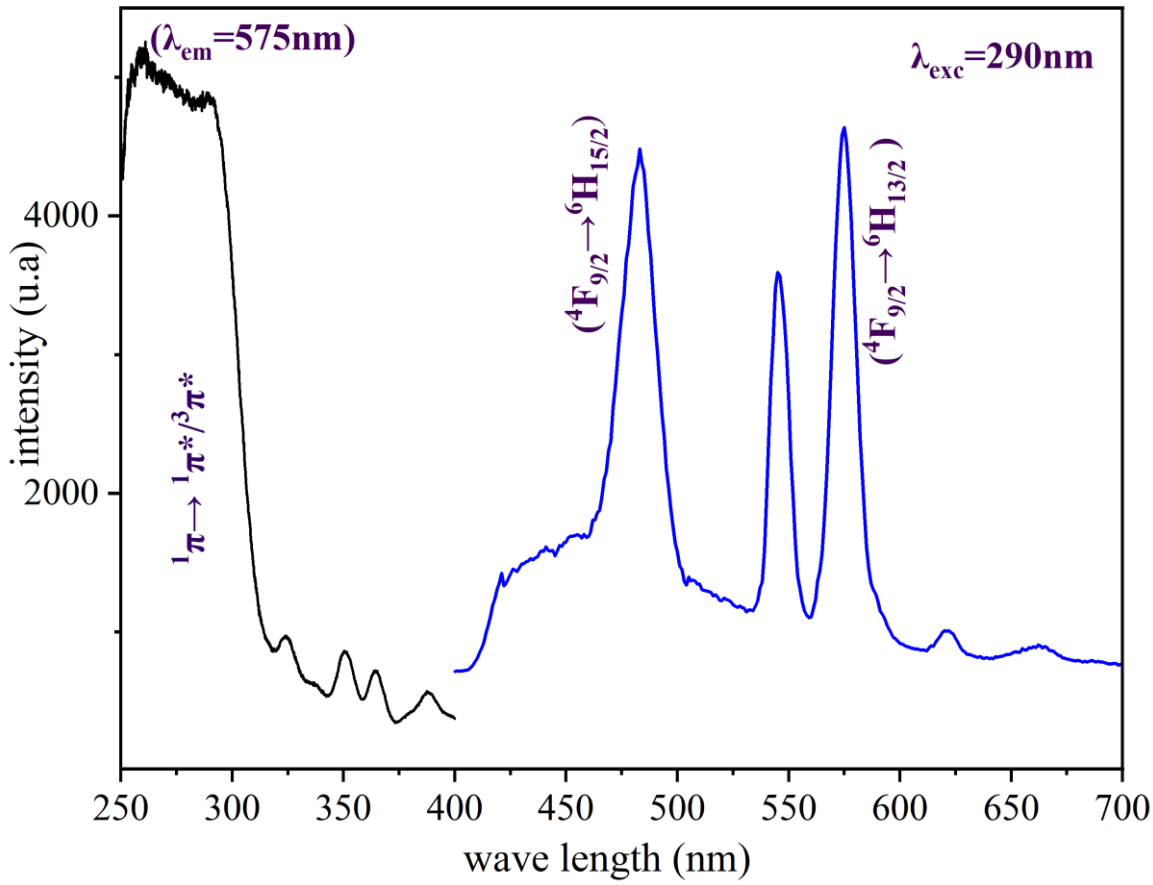

Figure 3. 20 Room temperature solid-state excitation (λ_{em} = 574 nm) and emission (λ_{exc} = 290 nm) spectra of Dy.

Room-temperature solid-state excitation and emission spectra of Tb complex in series 2 is presented in (**Figure 3. 21**) at λ_{em} = 545 nm and λ_{exc} = 290nm. The excitation spectrum displays a broad band at 270 nm attributed to the $^1\pi \rightarrow {}^1\pi^*/{}^3\pi^*$ transitions characteristic of isophthalic ligand indicating that this ligand exhibits an effective antenna effect in this compound.

Upon excitation at 290 nm show emission peaks at 489 nm, 545 nm, 584 nm, 620 nm corresponding to $^5D_4 \rightarrow {}^7F_J$ (J = 6, 5, 4, 3) transitions respectively. The $^5D_4 \rightarrow {}^7F_5$ band is the most dominant one [37].

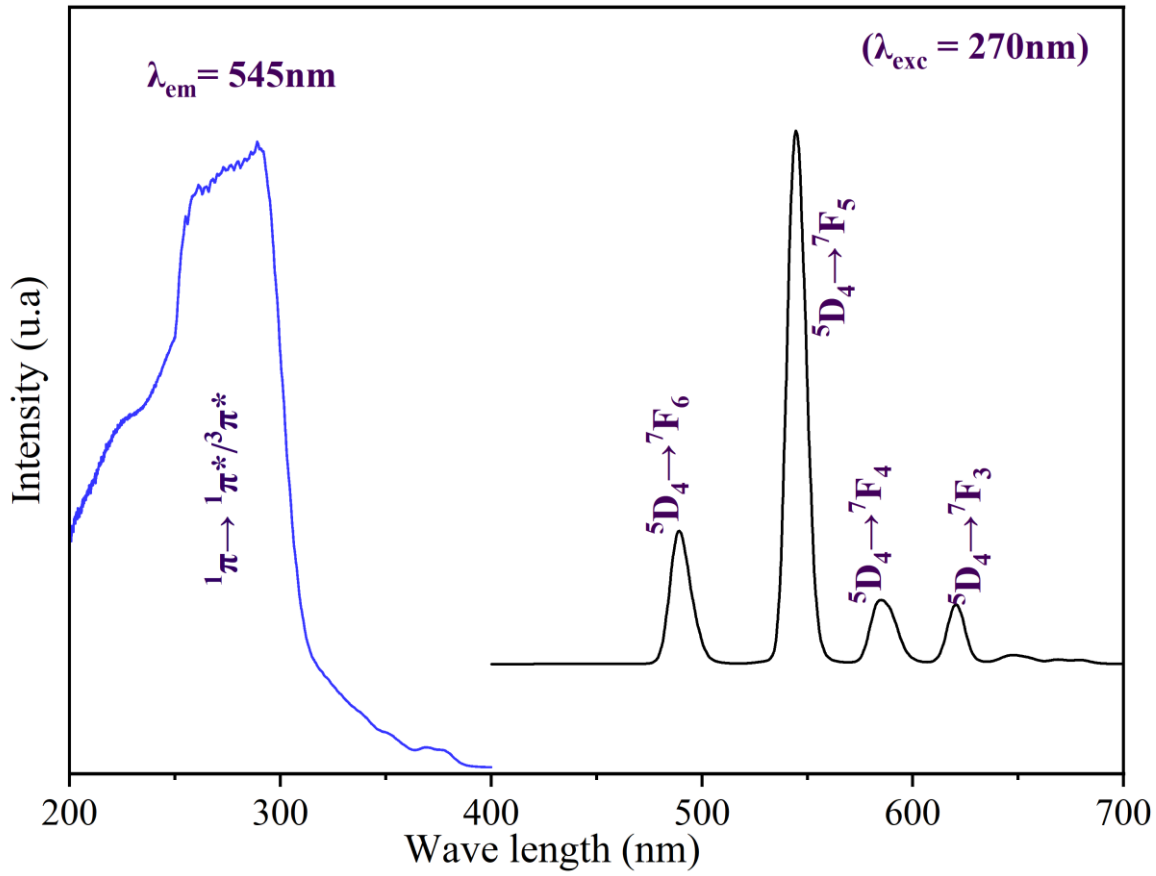

Figure 3. 21 emission and excitation spectra of Tb compound (λem=545nm, λexc=270nm).

3.3.3.3 Series 3

This series consists of a single coordination polymer incorporating dysprosium (Dy) as the metal center, also obtained from the first filtration.

3.3.3.3.1 Infra-Red Spectroscopy

The IR spectrum of the Dy-based compound is shown in **(Figure 3. 22)**. The analysis confirms the successful incorporation of both pimelic acid and isophthalic acid as ligands.

A broad band at 3347 cm^{-1} corresponding to ν(O-H) vibration band of water molecules. A weak band at 2996 cm^{-1} corresponds to aliphatic ν(C-H) stretching (methylene CH_2–) of pimelate.

The strong bands observed at 1600 and 1529 cm^{-1} for asymmetric COO^- stretching and 1454 and 1403 cm^{-1} for symmetric COO^- stretch confirm complete deprotonation of both pimelic and isophthalic acids. In this case the difference in ν_{as} (COO^-) and ν_s(COO^-) are 146 cm^{-1} and 126 cm^{-1} respectfully which suggest bridging coordination with the Dysprosium.

The band at 1162 cm^{-1} is ascribed to the ν (C–O) stretch in the dicarboxylate ligands, The out of plane bending band of the aromatic δ(C−H) at 744 cm^{-1} thus confirming Isophthalate. A band at 437cm^{-1} corresponds to ν(Ln–O) bond confirming the coordination of metal/ligands.

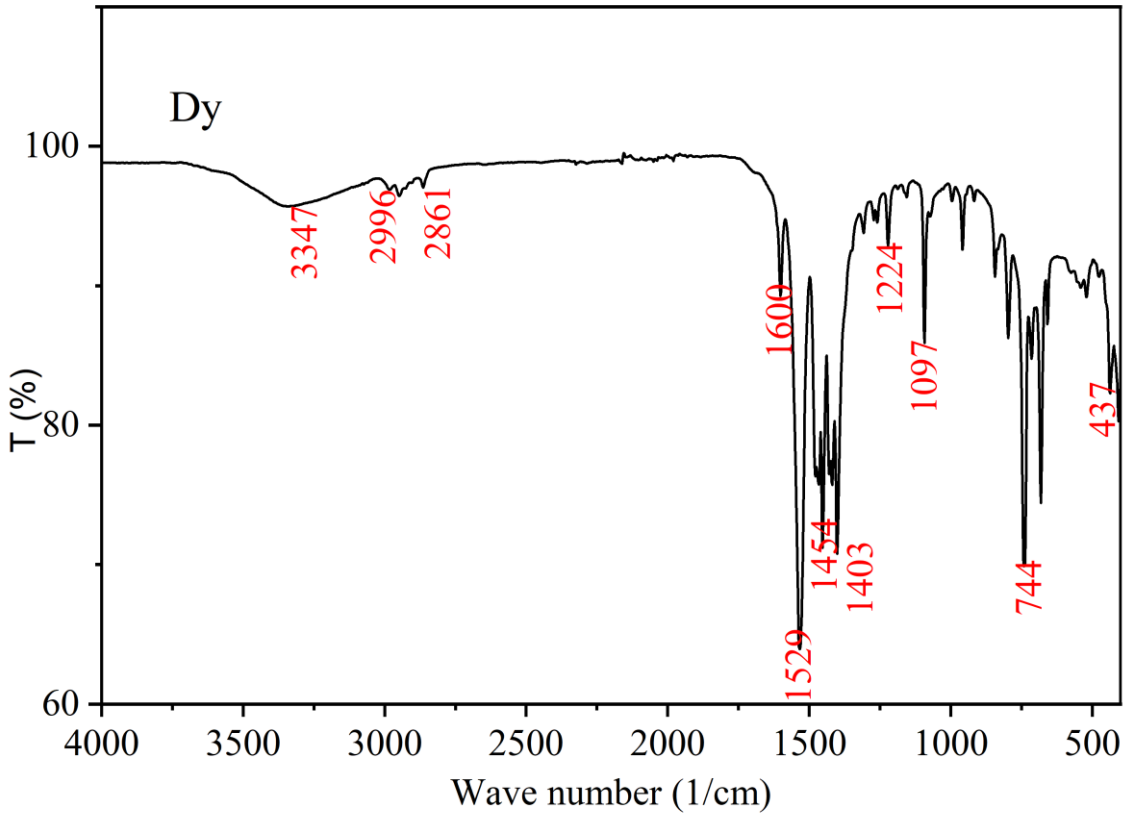

Figure 3. 22 infra-red spectrum of series 3.

3.3.3.3.2 Powder X Ray Diffraction on Serie 3

The powder XRD Pattern of Serie 3 (**Figure 3. 23**) gives sharp, defined peaks which indicate high crystallinity and purity of the compound.

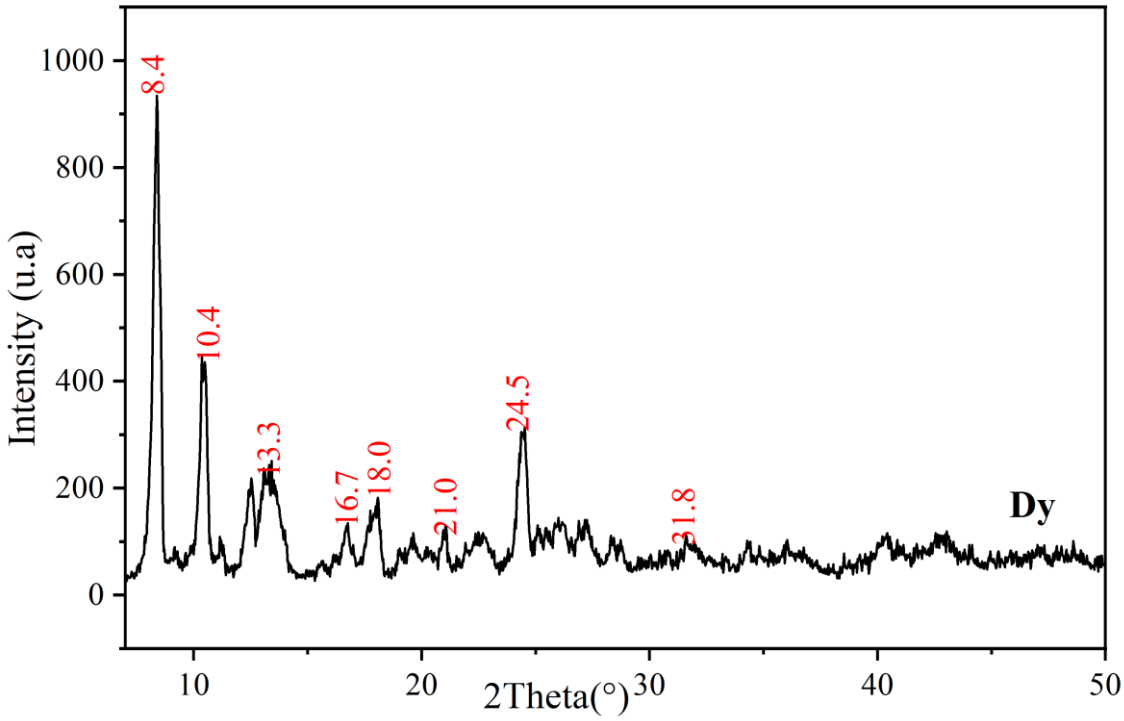

Figure 3. 23 The diffractogram of powder XRD of

3.3.3.3.3 Thermal analysis on series 3

The thermal behaviour of Series three compound was analysed by TGA and DSC. As seen in (**Figure 3. 24**) the compound undergoes a multi-step decomposition, indicating the sequential loss of water molecules and the breakdown of the organic ligand framework **(Table 3. 8)**. The final residue, stabilized after 600 °C, corresponds to the expected lanthanide oxide (Dy_2O_3).

Table 3. 8 thermal decomposition of series 3 compound.

Temperature range (°C)	**Weight loss (%)**	**DSC Observation**	**Assignment**
25.0 to 107.3	1.7	Endothermic peak at 59°C	Loss of hydration water
107.3 to 182.0	4.8	Endothermic peak at 164°C	Loss of coordinate water molecules
182.0 to 254.3	None	None	Stable intermediate
254.3 to 333.0	25.8	Endothermic peak at 318°C	Ligand decomposition

333.0 to 448.1	7.0	endothermic peak at 432°C	Continued ligand degradation
448.1 to 708.0	22.6	Endothermic peak at 608°C	Final ligand decomposition

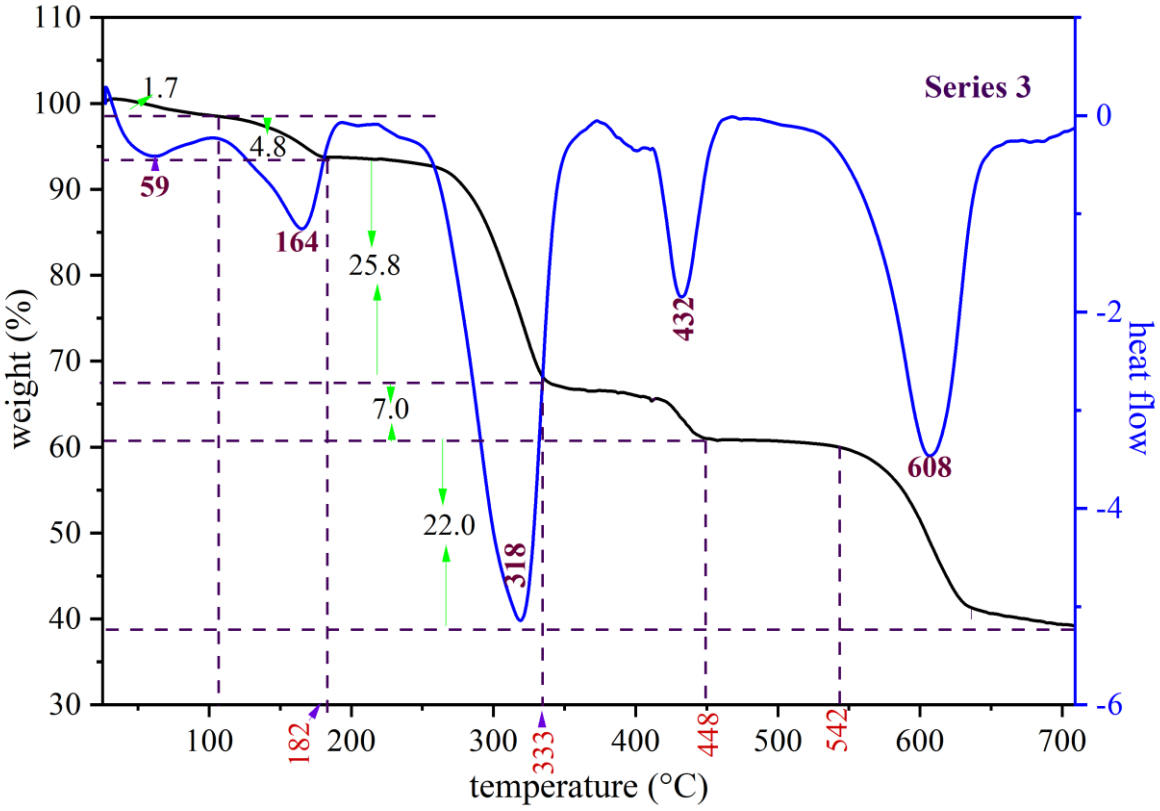

Figure 3. 24 TGA and DSC curves of the compound in Series 3 showing thermal decomposition behaviour from 25 °C to 708°C.

3.3.3.4 series 4

This comprises three lanthanide-based coordination polymers synthesized using lanthanum (La^{3+}), terbium (Tb^{3+}), and erbium (Er^{3+}) ions. These compounds were obtained through a combination of second and third hydrothermal filtrations, suggesting possible variations in crystallization kinetics and reaction conditions during the synthesis process. Despite the differing filtration steps, the coordination polymers isolated in this series exhibit consistent structural characteristics, as evidenced by their spectroscopic and crystallographic analyses.

3.3.3.4.1 Infra-red spectroscopy.

The FTIR spectra of the lanthanide-based coordination polymers in Series 4 (La, Tb, Er) are shown in (**Figure 3. 25)**. The spectra reveal a series of characteristic absorption band corresponding to both the organic ligands (Isophthalate and pimelate) and metal–ligand coordination, with all three complexes exhibiting largely similar profiles, indicative of isostructurality.

Abroad band at 3544cm^{-1} is attributed to the ν(O–H) stretching vibrations. This arises from lattice water molecules and the broad band 2500–3000 cm^{-1} corresponds to the ν(O–H) of residual uncoordinated carboxylic acid groups. The weak intensity bands 2964 cm^{-1} is associated with aliphatic ν(C–H) stretching vibrations of methylene (–CH_2–) groups. These are characteristic of the aliphatic chain present in pimelate.

A sharp peak at 1729 cm^{-1} corresponds to the C=O stretching vibration of COOH group, suggesting incomplete deprotonation. The characteristic peaks of functional group COO^- of the deprotonated dicarboxylic acid at 1673 cm^{-1} for asymmetric vibrations and at 1434 cm^{-1} for symmetric vibrations [78].

Multiple bands in the region 1297 to 1145 cm^{-1} arise from C–O stretching vibrations. The band at 725 represents corresponds to the out-of-plane bending of aromatic C–H groups. The band appearing in the low-frequency region at 484 cm^{-1} is assigned to (Ln–O) stretching vibrations. This is direct evidence of coordination between the lanthanide ion and the oxygen atoms of the carboxylate groups from both pimelic and isophthalic acids [71].

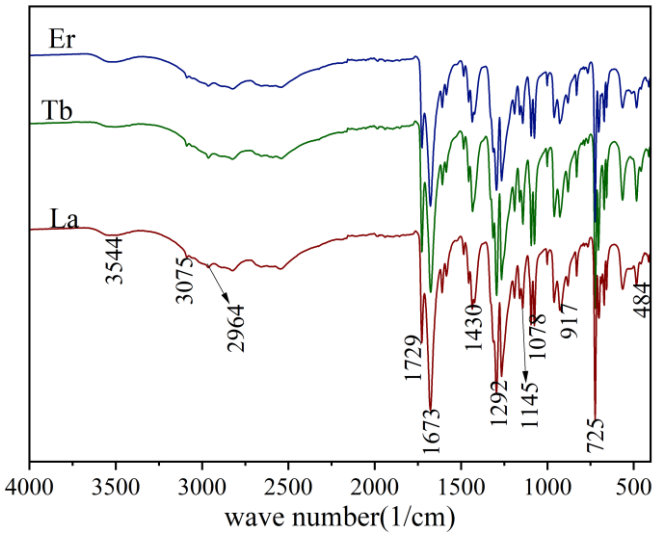

Figure 3. 25 infra-red spectrum of Serie 4 complex.

3.3.3.4.2 Powder X Ray Diffraction on Serie 4

The powder X-ray diffraction (PXRD) patterns of the lanthanide coordination polymers containing Er, Tb, and La in Series 4 exhibit highly consistent and sharp diffraction peaks (**Figure 3. 26**). The identical peak positions across the three complexes strongly suggest that the compounds are isostructural, with a shared crystalline framework. This structural similarity indicates that the coordination environment and topology are primarily dictated by the organic ligands, despite the differing ionic radii of the lanthanide centers. The presence of sharp and well-defined reflections confirms the high crystallinity and phase purity of the synthesized materials.

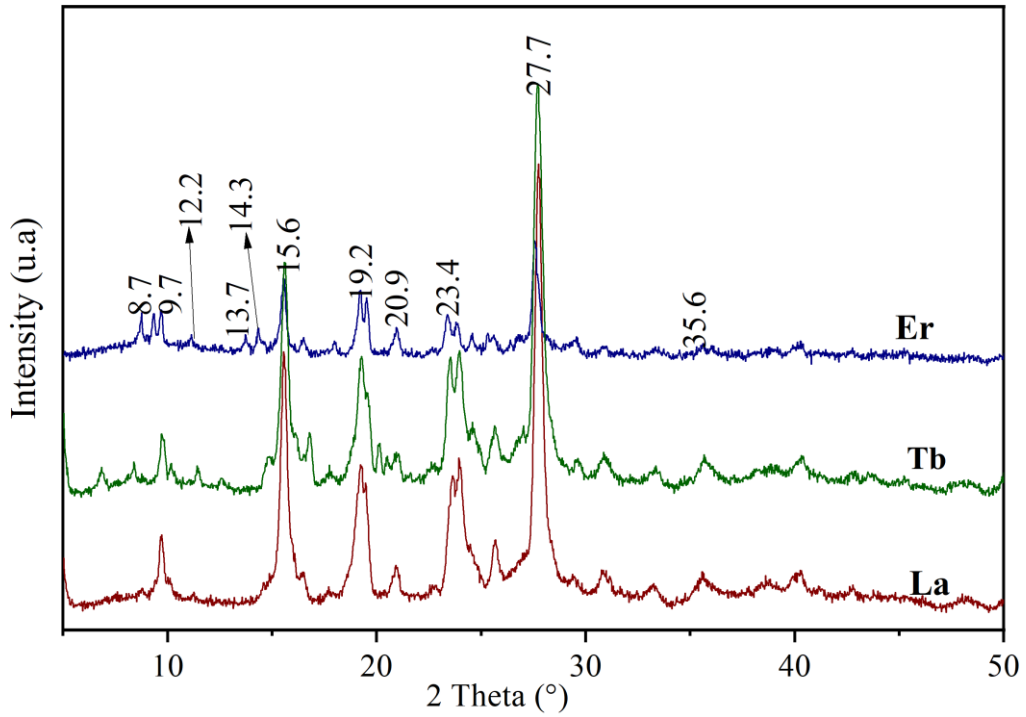

Figure 3. 26 PXRD of series 4.

We were not able to carry out further analysis (thermal analysis and photoluminescence) on this series because of the quantity of the sample was limited.

3.3.3.5 Series 5

Series 5 consists of coordination polymers incorporating two lanthanide metals erbium (Er) and ytterbium (Yb). These complexes were obtained from the first hydrothermal filtration and their structural and spectroscopic features indicate a high degree of uniformity.

3.3.3.5.1 Infra-red spectroscopy

The Fourier-transform infrared (FTIR) spectra of the Series 5 compounds **(Figure 3. 27)** confirm coordination of the lanthanide ions with the dicarboxylate ligands.

A broad band at 3257-3623 cm^{-1} is attributed to the ν(O–H) stretching vibrations that arises from lattice water molecules. A weak band at 3080 cm^{-1} assigned to the elongation vibration band of the aromatic ν(C-H) bond. The characteristic peaks of functional group COO^- of the deprotonated dicarboxylic acid at 1604 cm^{-1} and 1525 cm^{-1} for asymmetric vibrations and at 1448 cm^{-1} and 1382 cm^{-1} for symmetric vibrations, ($\Delta\nu_1$ = 156 cm^{-1} $\Delta\nu_2$ = 143 cm^{-1}). These values typically suggest a chelating or bridging coordination mode of the carboxylate groups in metal ligand frameworks.

The intense peak at 711 cm^{-1} corresponds to the out of plane bending band of the aromatic δ(C−H) thus confirming isophthalic acid. The peak at 447 cm^{-1} is assigned to (Ln–O) stretching vibrations confirming the coordination of Ln to the organic ligands.

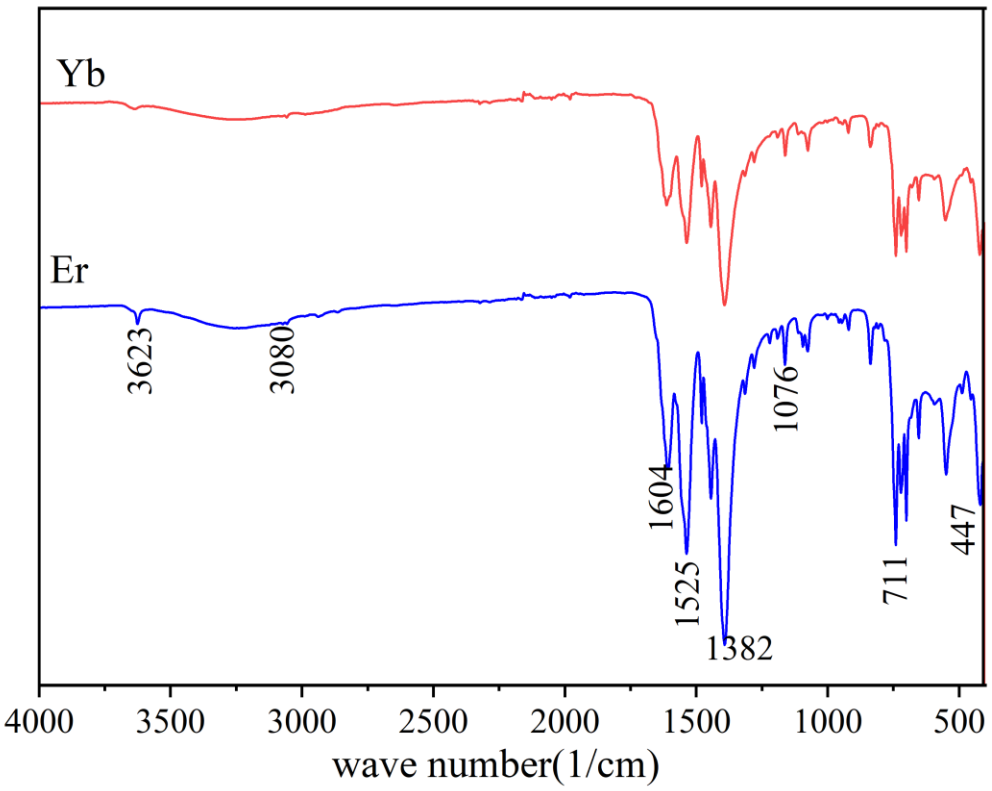

Figure 3. 27 Infra-red spectrum of series 5.

3.3.3.5.2 Powder X Ray Diffraction on Serie 5

The PXRD patterns of the Er and Yb coordination polymers in Series 5 **(Figure 3. 28**) display similar diffraction features confirming their isostructural nature. The sharp, well-resolved peaks are indicative of crystalline, single-phase materials. A comparative analysis with known structures in the literature reveals a high degree of structural similarity with the $[Ln_2(ip)_3(H_2O)_2]_n$ framework (Ln = La, Gd, Nd, Sm, Eu, Tb and ip= 1,3-benzenedicarboxylate), as shown in (**Figure 3. 29**). This structural resemblance highlights the robustness of the coordination framework across different lanthanide ions and suggests that the organic ligand plays a dominant role in dictating the overall architecture [56, 57, 58, 59, 60].

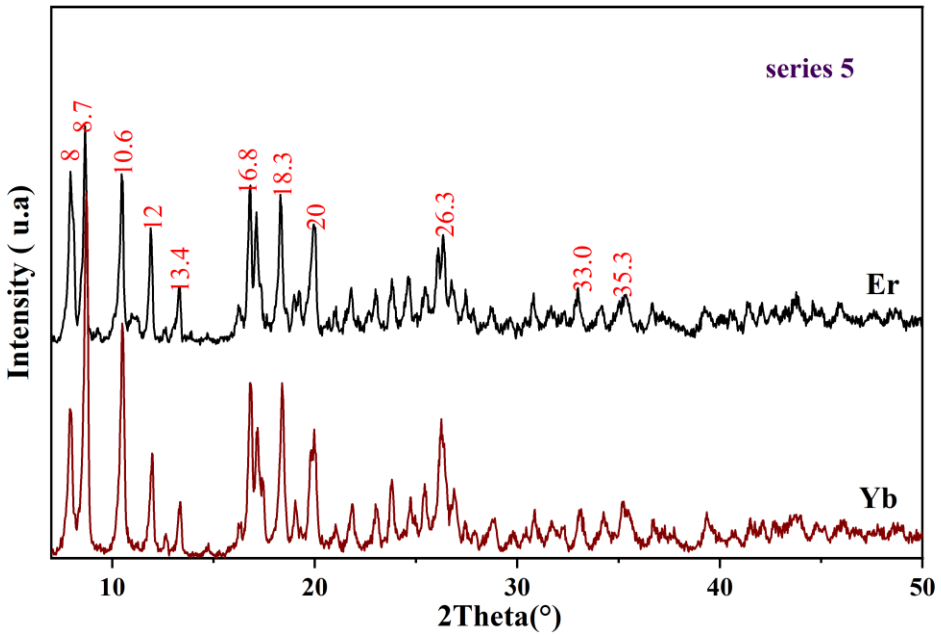

Figure 3. 28 XRD diffractogram of Serie 5.

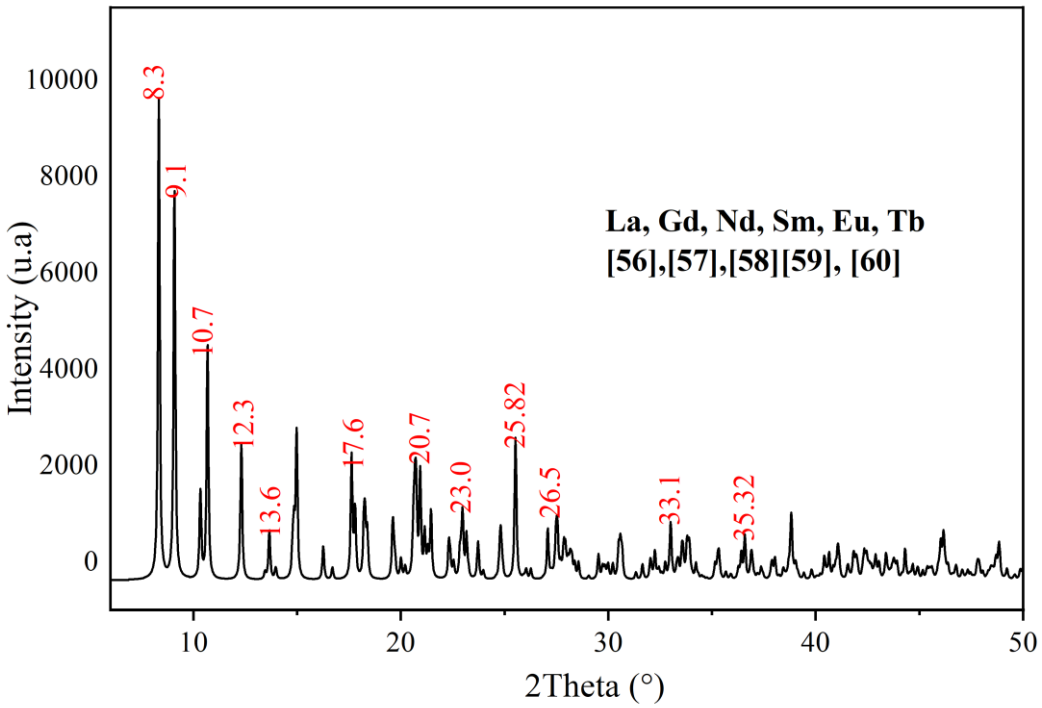

Figure 3. 29 DRX diffractogram of $[Ln_2(ip)_3(H_2O)_2]$ n.

3.3.3.5.3 Thermal analysis

The thermal behaviour of Series five compound was analysed by TGA and DSC. As seen in **(Figure 3. 30)**, the compound undergoes a multi-step decomposition, indicating the sequential loss of water molecules and the breakdown of the organic ligand framework (**Table 3. 9**).

Table 3. 9 interpretation of thermal decomposition of series 5.

Temperature range (°C)	**Weight loss (%) experimental**	**DSC Observation**	**Assignment**
45.3 to 165.2	7.0	Endothermic peak at 133°C	Loss of coordination water molecules
165.2 to 458.0	None	none	Stable intermediate
458.0 to 708.0	39.3	Endothermic peak at 605°C	Ligand decomposition

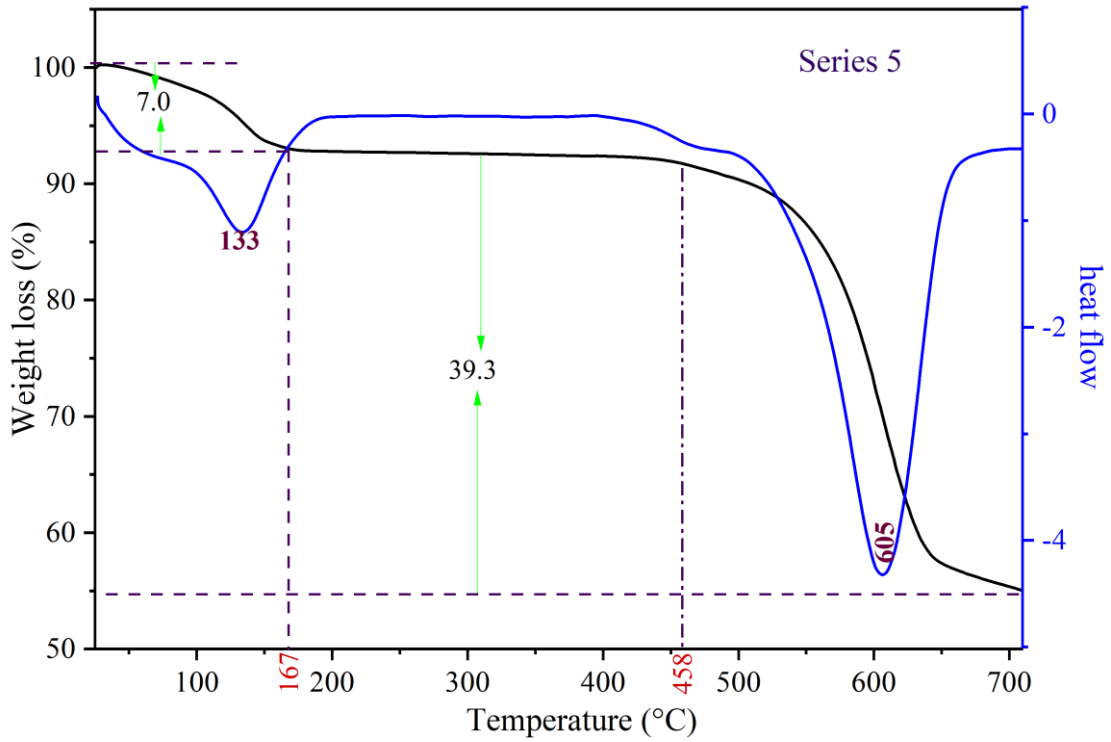

Figure 3. 30 interpretation of thermal decomposition of series 5.

3.3.3.6 Series 6

This series comprises two coordination polymers incorporating Dysprosium (Dy) and Terbium (Tb) as the central metal ions. These complexes were obtained from the first hydrothermal filtration.

3.3.3.6.1 Infra-red spectroscopy.

The FTIR spectra of the two coordination polymers in Series 6 are identical to each other as observed in **(Figure 3. 31)**.

A broad band at 3243 cm^{-1} is attributed to the v (O–H) stretching vibrations that arises from lattice water molecules. The characteristic peaks of functional group COO^- of the deprotonated dicarboxylic acid at 1612 cm^{-1} and 1527 cm^{-1} for asymmetric vibrations and at 1448 cm^{-1} and 1348 cm^{-1} for symmetric vibrations, ($\Delta\bar{\upsilon}_1$ = 164 cm^{-1} $\Delta\bar{\upsilon}_2$ = 179 cm^{-1}). These values typically suggest a chelating or bridging coordination mode of the carboxylate groups in metal ligand frameworks.

The intense peak at 717cm^{-1} corresponds to out of plane bending band of the aromatic δ(C−H) thus confirming isophthalic acid. The peak at 422 cm^{-1} is assigned to (Ln–O) stretching vibrations confirming the coordination of Ln to the organic ligands.

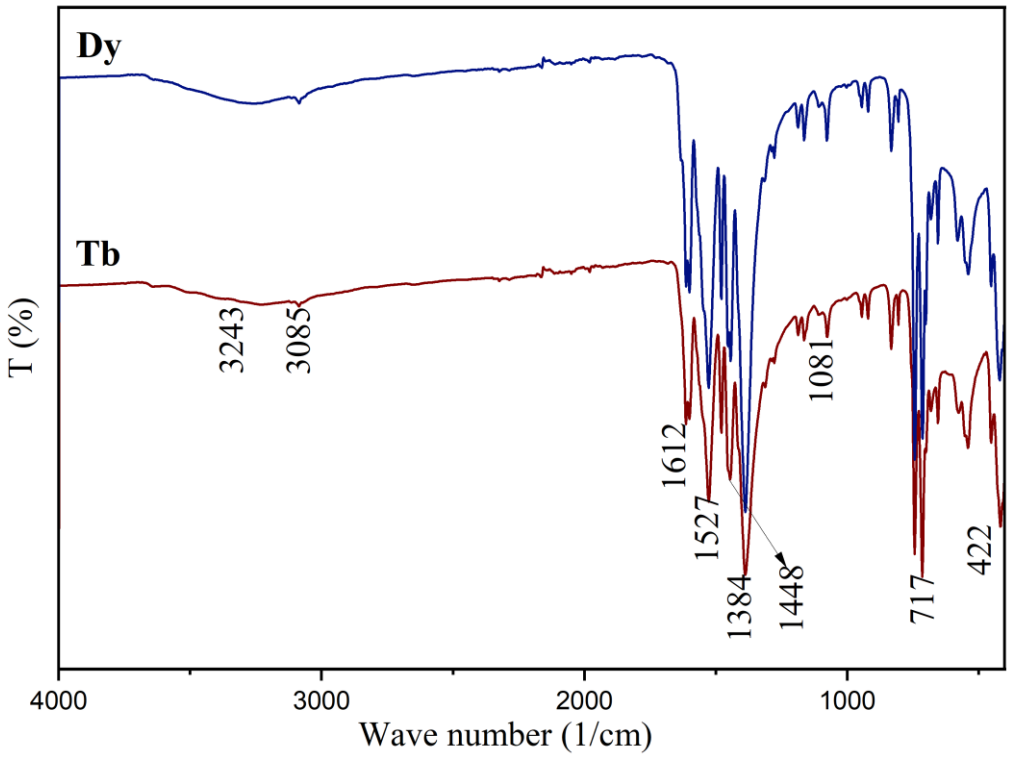

Figure 3. 31 Infra-red spectra of series 6.

3.3.3.6.2 Powder X Ray Diffraction

The PXRD patterns **(Figure 3. 32)** of the Series 6 compounds exhibit sharp and well-defined peaks, indicative of highly crystalline materials. The similarity in the profiles supports the formation of isostructural frameworks involving Dy and Tb ions.

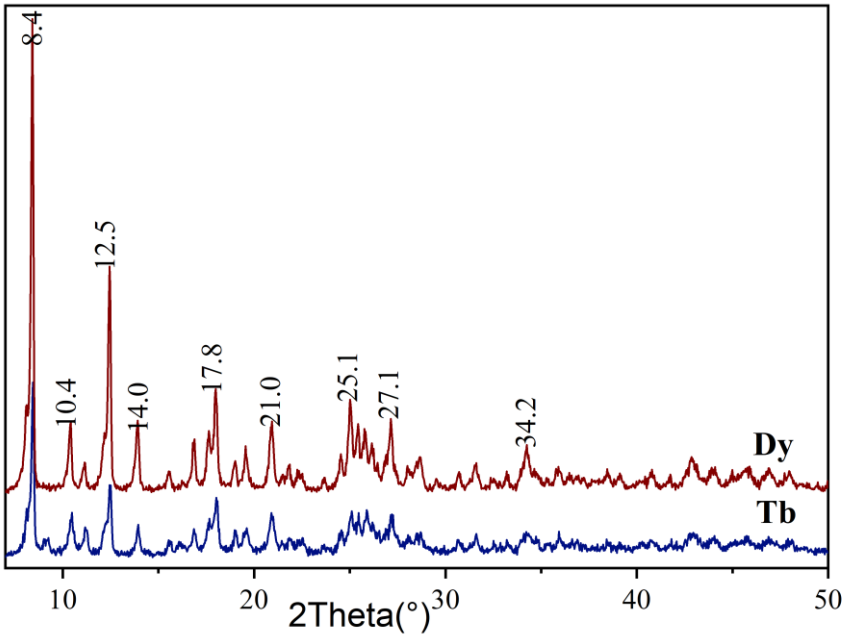

Figure 3. 32 PXRD pattern of series 6.

Comparison with literature data reveals that the diffraction patterns are isostructural to those reported for the compound $[Ln_2(ip)_3(H_2O)_2]. nH_2O$ in (**Figure 3. 33**) where ip denotes Isophthalate [64, 66, 65].

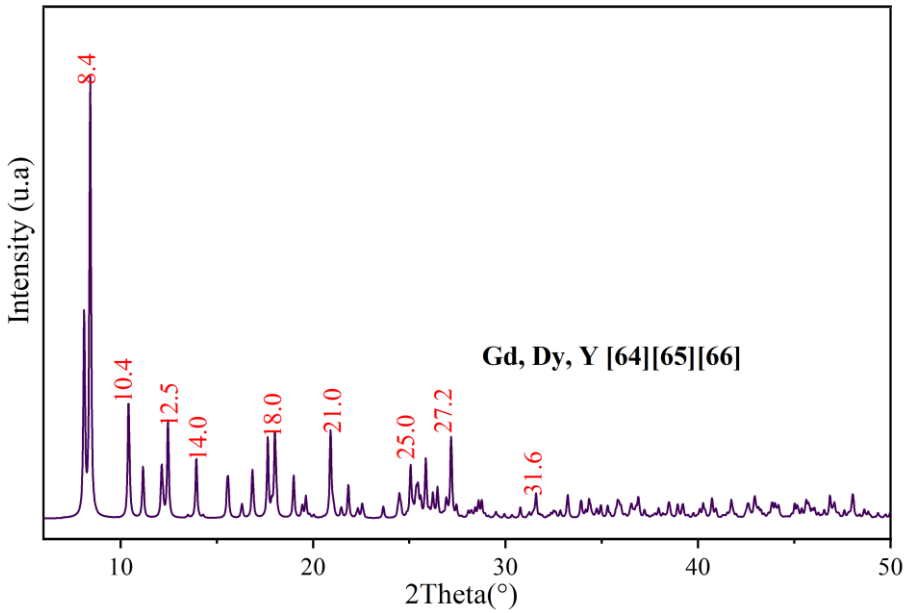

Figure 3. 33 Diffractogram of $[Ln_2(ip)_3(H_2O)_2]. nH_2O$.

3.3.3.6.3 Photoluminescence analysis

The luminescent properties of series 6 were investigated on solid state samples of Dy, and Tb complexes at room temperature.

The emission and excitation spectra of Tb in series 6 upon excitation at 259 nm and emission at 545nm is displayed in (**Figure 3. 34**). The excitation spectrum displays a broad band at 259 nm attributed to the $^{1}\pi \rightarrow {}^{1}\pi^{*}/{}^{3}\pi^{*}$ transitions characteristic of isophthalic ligand indicating that this ligand exhibits an effective antenna effect in this compound.

The emission spectrum shows three characteristic emission lines of Tb (III) at 488 nm, 545 nm, 585 nm and 620 nm resulting from $^{5}D_4 \rightarrow {}^{7}H_6$, $^{5}D_4 \rightarrow {}^{7}H_5$, $^{5}D_4 \rightarrow {}^{7}H_4$ and $^{5}D_4 \rightarrow {}^{7}H_3$ respectively.

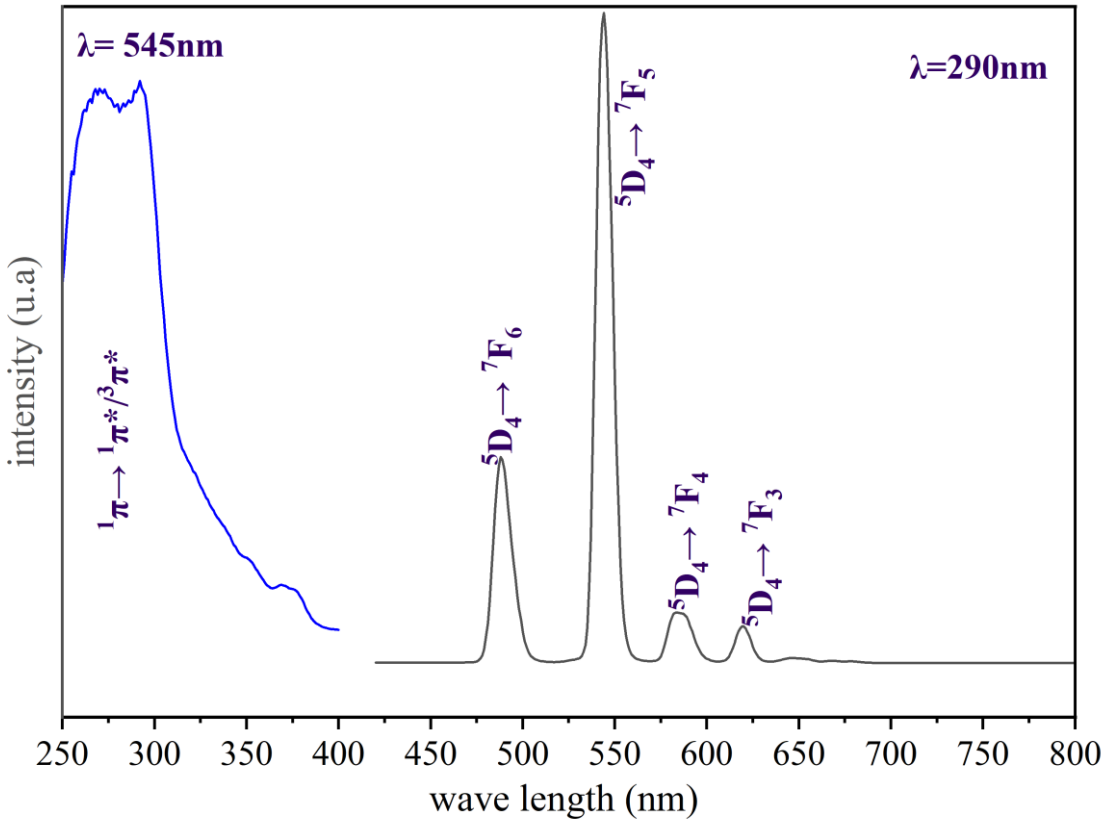

Figure 3. 34 The photoluminescence spectra of the Tb compound in series 6

3.3.3.7 Serie 7

This series consists of a single coordination polymer incorporating Ytterbium (Yb) as the central metal ion also obtained from the first hydrothermal filtration.

3.3.3.7.1 Infra-red spectroscopy

The FTIR spectrum of the Yb coordination polymer in this series confirms coordination through carboxylate groups (**Figure 3. 35**). A weak band between 3629 cm^{-1} is attributed to the ν(O–H) stretching vibrations of lattice water molecules and the broad band 2500–3000 cm^{-1} corresponds to the ν(O–H) of residual uncoordinated carboxylic acid groups. The weak intensity bands 3070 cm^{-1} attributed to the ν(C–H) stretching and a strong band at 742 cm^{-1} corresponds to δ(C−H) out of plane bending vibrations of the aromatic function in isophthalate.

A sharp peak at 1656 cm^{-1} corresponds to the C=O stretching vibration of undissociated carboxylic acid, suggesting incomplete deprotonation. The characteristic peaks of functional group COO^- of the deprotonated dicarboxylic acid at 1602 cm^{-1} and 1536 cm^{-1} for asymmetric vibrations and at 1444 cm^{-1} and 1392 cm^{-1} for symmetric vibrations ($\Delta\bar{\upsilon}_1$=158 and $\Delta\bar{\upsilon}_2$= 144) which suggests bridging coordination mode.

Multiple bands in the region 1300–1000 cm^{-1} arise from C–O stretching vibrations and in-plane bending of aromatic C–H bonds. A band appearing in the low-frequency region at 422 cm^{-1} are assigned to (Yb–O) stretching vibrations. This is evidence of coordination between the lanthanide ion and the oxygen atoms of the carboxylate group of Isophthalate.

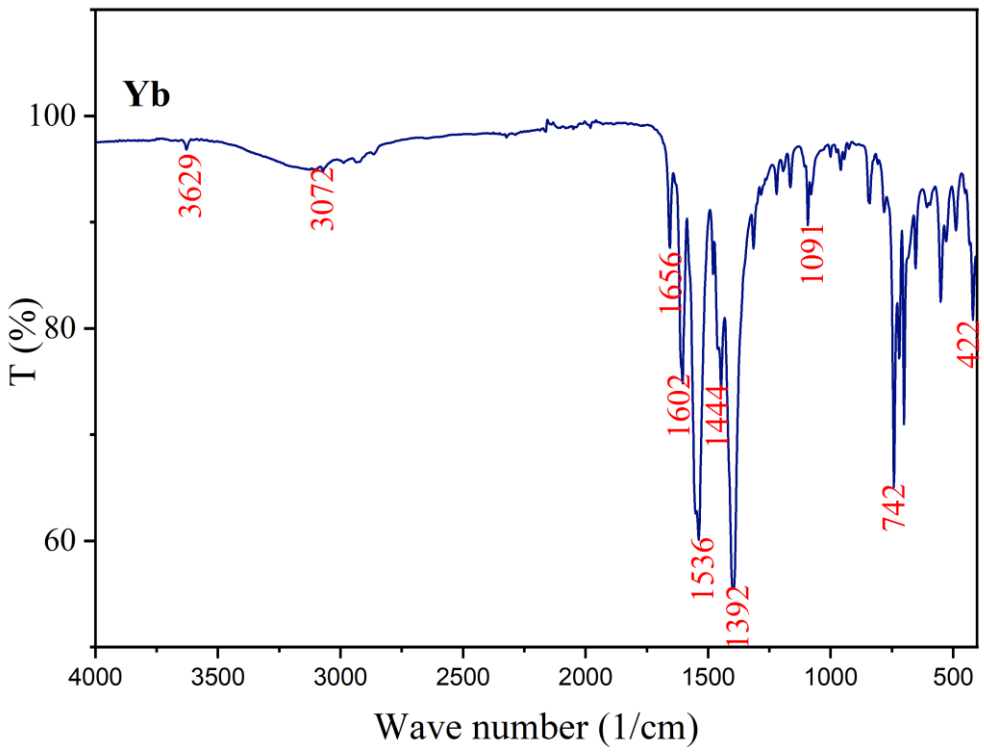

Figure 3. 35 The FTIR spectrum of the Yb complex in series 7.

3.3.3.7.2 Powder X Ray Diffraction

The PXRD pattern of the Yb-based coordination polymer in this series 7 displays well-defined and sharp peaks (**Figure 3. 36)**, indicating the crystalline nature of the compound, he sharp and intense peaks further indicate that the compound is pure-phase, with no detectable amorphous content or secondary phases.

After comparing it with existing literature, the PXRD of Serie 7 is similar to that of $[Nd_2(ip)_2(Hip)_2(H_2O)]_n . nH_2O$ (ip = isophthalic acid) (**Figure 3. 37**) [63, 64].

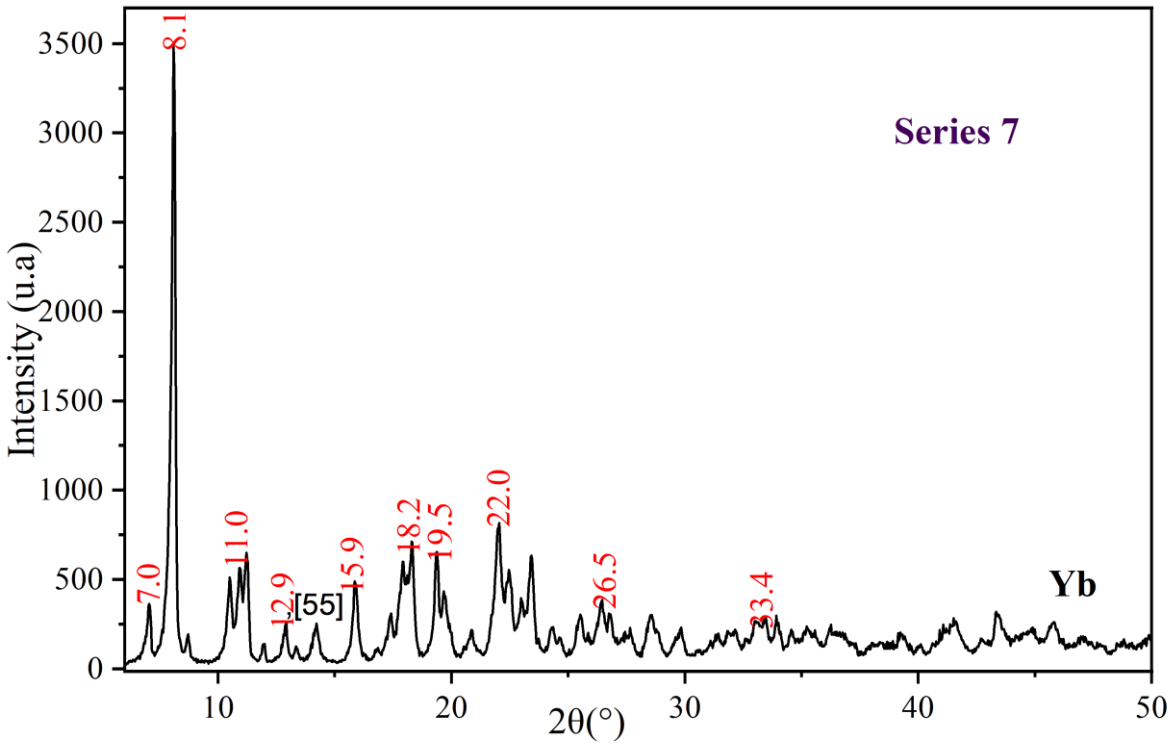

Figure 3. 36 The PXRD pattern of the Yb-based coordination polymer in series 7.

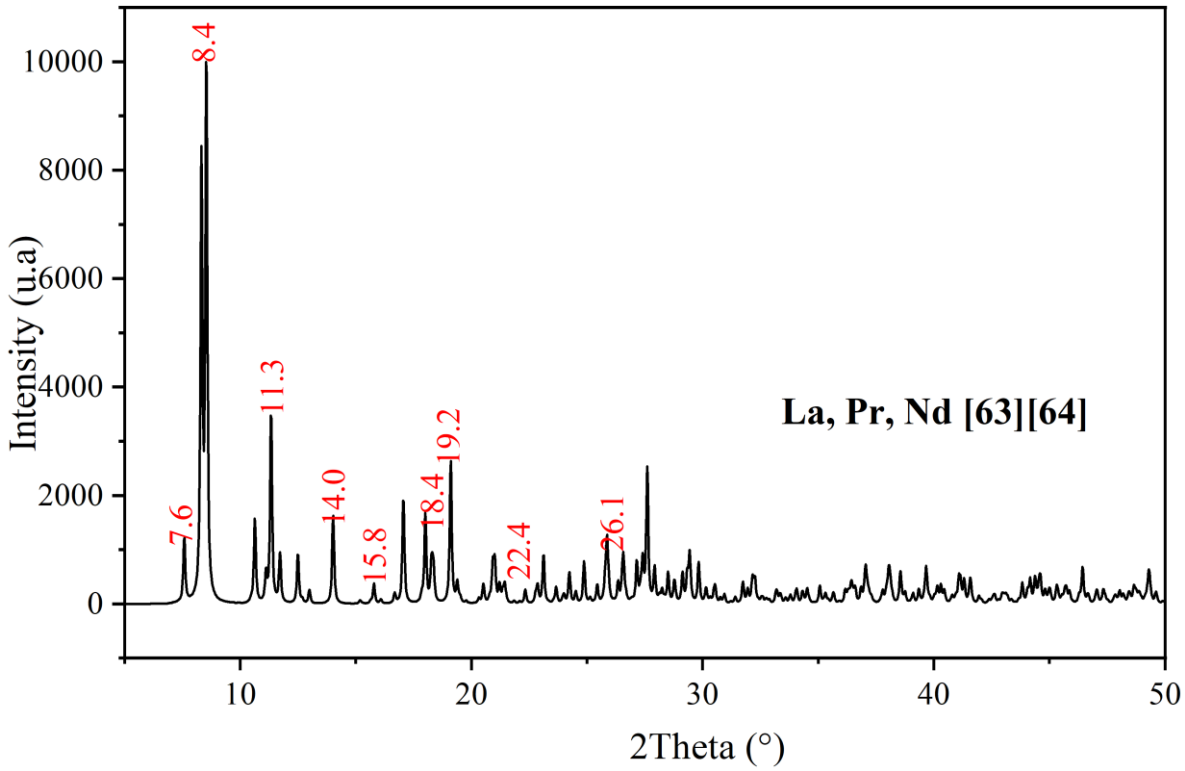

Figure 3. 37 The PXRD pattern of $[Nd_2\ (ip)_2\ (Hip)_2(H_2O)]_n.\ nH_2O$ (ip = isophthalic acid).

3.3.3.7.3 Thermal analysis

The thermal behaviour of the yttrium-based coordination polymer 7 was examined using TGA and DSC. As seen in (**Figure 3. 38**), the compound undergoes a multi-step decomposition given in (**Table 3. 10**).

Table 3. 10 interpretation of thermal decomposition of series 7.

Temperature range (°C)	**Weight loss (%) experimental**	**DSC Observation**	**Assignment**
48.9 to 120.2	2.7	Endothermic peak at 66°C	Loss of Hydration water molecules
120.2 to 327.0	0.9	Endothermic peak at 307°C	Loss of coordination water molecules
327.0 to 412.3	None	none	Stable intermediate
412.3 to 519.0	12.9	Endothermic peak at 470°C	Ligand decomposition
519.0 to 708.0	24.4	Endothermic peak at 604°C	Ligand decomposition

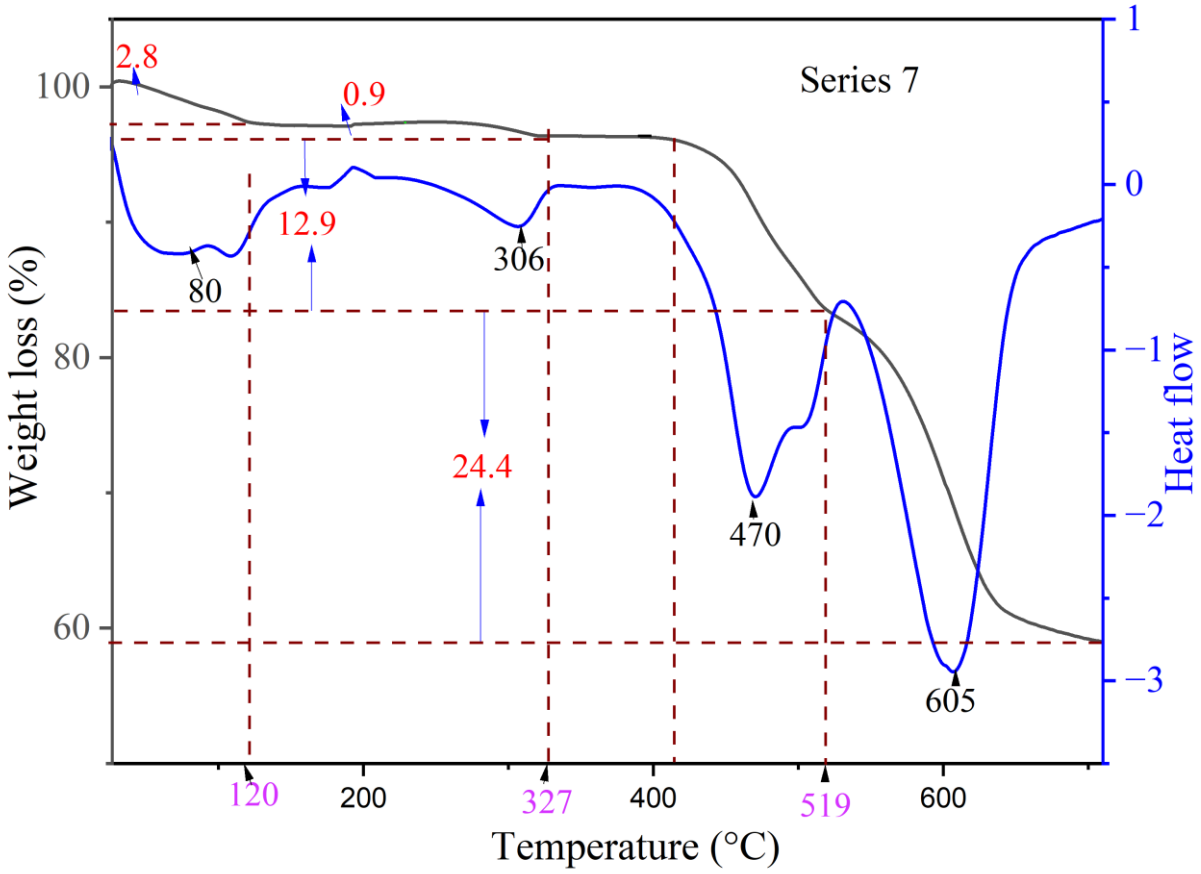

Figure 3. 38 The thermal decomposition curves (TGA and DSC) of series 7.

General Conclusion

General conclusion

This research successfully explored the synthesis and characterization of lanthanide-based coordination polymers, using both rigid (isophthalic acid) and flexible (pimelic acid) dicarboxylic ligands to generate diverse structural frameworks with potential photoluminescent properties.

Two synthetic strategies were employed: the hydrothermal method, and the slow diffusion method. Hydrothermal synthesis resulted into the formation of well-defined crystalline products by varying temperature, reaction time, and metal-to-ligand ratios. A total of seven compound series (series 1 to 7) were obtained.

Hydrothermal products were characterized by infrared spectroscopy and powder X-ray diffraction (PXRD). PXRD analysis enabled the identification of structural differences across the series. Comparison with simulated patterns from literature data revealed that series 1 to 4 appear to be novel structures while series 5 to 7 are isostructural analogs of known compounds with different lanthanide ions.

Thermal stability was assessed using TGA and DSC, confirming multistep decomposition and the formation of Ln_2O_3 as the final residue.

The photoluminescent behaviour of selected compounds was investigated in the visible range, with Tb, Dy and Sm compounds showing promising emission characteristics, making them potential candidates for optical or sensing applications.

Crystals obtained from the slow diffusion method were also analysed. IR spectroscopy indicated that many matched the spectrum of uncoordinated isophthalic acid, suggesting that coordination did not occur effectively under those conditions. However, the block-like crystals obtained show promise for SCXRD analysis. Unfortunately, due to limited equipment access, single-crystal X-ray diffraction could not yet be performed, though collaborations are being sought to complete this essential structural analysis.

The results presented in this study establish a solid foundation for the development of luminescent lanthanide coordination polymers. Future efforts will focus on

- optimizing both synthesis methods, especially slow diffusion, to favour successful coordination.
- Performing SCXRD to determine the exact structures of the new compounds.
- Enhancing photoluminescent performance through further ligand design and metal variation.

General conclusion

This work contributes to the broader understanding of how ligand flexibility influences the architecture and properties of lanthanide-based materials, paving the way for future development of functional coordination networks in advanced materials science.

Bibliographic references

Bibliographic References

[1] S. Kitagawa and S. Noro, "'Coordination Polymers: Infinite Systems', Compr. Coord. Chem. II," pp. 231–261, 2003.

[2] J. L. C. Rowsell and O. M. Yaghi, "Metal-organic frameworks: A new class of porous materials", Microporous Mesoporous Mater.," vol. 73, pp. 3–14, 2004.

[3] M. Ataro Rezaei and N. Rabiee, "'Green Metal-Organic Frameworks (MOFs) for Biomedical Applications', Microporous Mesoporous Materials," vol. 335, p. 111670, 2022.

[4] W. Levason, "Chemistry and applications of the lanthanides," Coord. Chem. Rev, vol. 340, p. 1, 2017.

[5] J. C. G. Bünzli and S. V. Eliseeva, "'Basics of Lanthanide Photo physics,' In Lanthanide Luminescence, Springer Series on Fluorescence, vol. 7, Springer, Berlin, Heidelberg," pp. 1–45, 2010.

[6] Guillou. J. Wang, "Multi-Emissive Lanthanide-Based Coordination Polymers for Potential Application as Luminescent Bar-Codes," Inorg. Chem., vol. 58, pp. 2659–2668, 2019.

[7] B. Benmerad, "Cristallogenèse et études structurales de nouveaux dicarboxylâtes de lanthane (III), Université des sciences et de la technologie Houari Boumediene," 2000.

[8] B. Cornils and P. Lappe, "Dicarboxylic Acids, Aliphatic, Ullmann's Encycl. Ind. Chem," 2000.

[9] G. B. Kauffman, "Theories of Coordination Compounds," in Alfred Wener's triumph In Coordination Chemistry, Washington DC, 1994, pp. 2–33.

[10] E. C. Constable and C. E. Housecroft, "Coordination chemistry: The scientific legacy of Alfred Werner," Chem Soc Rev, vol. 42, no. 4, pp. 1429–1439, 2013.

[11] S. F. A. Kettle, "Physical Inorganic Chemistry: A coordination chemistry approach," London, 1996.

[12] M. L. Tong and X. M. Chen, "Synthesis of Coordination Compounds and Coordination Polymers," in Modern Inorganic Synthetic Chemistry: Second Edition, Guangzhou, 2017, pp. 189–217.

[13] A. G. S. Catherine E. Housecroft, "Inorganic Chemistry second edition," England, 2005.

Bibliographic References

[14] J. A. McCleverty, Comprehensive coordination chemistry II. Amsterdam, Elsevier, 2003.

[15] G. Wulfsberg, “Chimie Inorganique : Théories et applications, Dunod, Paris,” 2002.

[16] G. A. Lawrance, “Introduction to Coordination Chemistry,” Australia, 2010.

[17] P. A. J. R. Tina Shriver, “Inorganic Chemistry, fifth edition,” New York, 2010.

[18] X. M. Chen, “Assembly Chemistry of Coordination Polymers,” in Modern Inorganic Synthetic Chemistry, Elsevier, 2011, pp. 207–225.

[19] G. S. G. and D. H. B. "John C. B. G. B. Kauffman, father of coordination chemistry in the United States, vol. 128. 1993.

[20] A. Kuznetsova, V. Matveevskaya, D. Pavlov, A. Yakunenkov, and A. Potapov, “Coordination polymers based on highly emissive ligands: Synthesis and functional properties,” Materials, vol. 13, no. 12, pp. 1–67, 2020.

[21] " A. Y. Robin and K. M. Fromm, “Coordination polymer networks with O- and N donors: What they are, why and how they are made",” vol. 250, pp. 2127–2157, 2006.

[22] M. Lippi and M. Cametti, “‘Highly dynamic 1D coordination polymers for adsorption and separation applications,’” " Coord. Chem. Rev., vol. 430, 2021.

[23] Y. Cheddani et al., “Synthesis, structural characterization, molecular docking analysis and carbonic anhydrase IX inhibitory evaluations of novel cerium (III)-based MOF constructed from 1,10-phenanthroline and fumaric acid,” J. Mol. Struct, vol. 1312, 2024.

[24] M. N. Akhtar, Y. C. Chen, M. A. Aldamen, and M. L. Tong, “3D Oxalato-bridged lanthanide(iii) MOFs with magnetocaloric, magnetic and photoluminescence properties,” Dalton Transactions, vol. 46, no. 1, pp. 116–124, 2017.

[25] J. C. G. Bünzli, “Review: Lanthanide coordination chemistry: From old concepts to coordination polymers,” in journal of coordination chemistry, 2014, pp. 3706–3733.

[26] G. F. W. Gunn, “Rare earth elements, critical metals handbook,” 2014.

[27] C.-Hui. Huang, Rare earth coordination chemistry, fundamentals and applications. John Wiley & Sons, 2010.

[28] S. Cotton, “Lanthanide and Actinide Chemistry,” United Kingdom, 2006.

Bibliographic References

[29] W. F. Meggers, "'Electron configurations of rare earth elements', Science, no. 2733.," vol. 105, pp. 514–516, 1947.

[30] T. Moeller, "The Chemistry of The Lanthanides Pergamon texts in inorganic chemistry, Elsevier.," vol. 26, pp. 1–101, 1973.

[31] D. F. Shriver and P. W. Atkins, "Chimie Inorganique, De Boeck," 2001.

[32] Stephen B. Castor and James B. Hedrick, "'Rare Earths', industrial minerals and rocks," pp. 769–792, 2006.

[33] J. G. Bünzli, "Lanthanides," in Kirk-Othmer Encyclopaedia of Chemical Technology, Wiley, 2013, pp. 1–43. [Online]. Available: https://onlinelibrary.wiley.com/doi/10.1002/0471238961.1201142019010215.a01.pub3

[34] J. C. G. Bünzli and C. Piguet, "Taking advantage of luminescent lanthanide ions," 2005.

[35] J. C. G. Bünzli, "On the design of highly luminescent lanthanide complexes," 2015, Elsevier.

[36] S. P. Bera, A. Mondal, and S. Konar, "Lanthanide Based Layer Type Two - Dimensional Coordination Polymers Featuring Slow Magnetic Relaxation, Magnetocaloric Effect and Proton Conductivity," Chem Asian J, vol. 14, no. 20, pp. 3702–3711, 2019.

[37] C.-Hui. Huang, Rare earth coordination chemistry, fundamentals and applications. John Wiley & Sons, 2010.

[38] R. D. H. J. E. M. and A. S. C. J. Andres, "A new anti-counterfeiting feature relying on invisible luminescent full colour images printed with lanthanide-based inks," Adv. Funct. Mater., vol. 24, no. 32, pp. 5029–5036, 2014.

[39] J. C. G. Bünzli, "Lanthanide luminescence for biomedical analyses and imaging," Chem Rev, vol. 110, pp. 2729–2755, 2010.

[40] D. L. and D. B. L. R. J. Roberts, ""Color-Tunable and White-Light Luminescence in Lanthanide-Dicyanoaurate Coordination Polymers," Inorg. Chem, vol. 56, no. 14, pp. 7948–7959, 2017.

[41] K. Nomiya, S. Takahashi, R. Noguchi, S. Nemoto, T. Takayama, and M. Oda, "Synthesis and characterization of water-soluble silver (I) complexes with L-histidine and (S)-(-)-2-pyrrolidone-5-carboxylic acid (H2pyrrld) showing a wide spectrum of effective

antibacterial and antifungal activities. Crystal structures of chiral helical polymers in the solid state," Inorg Chem, vol. 39, no. 15, pp. 3301–3311, 2000.

[42] P. Maestro et P. Dougier, "Les Terres rares dans les applications de la luminescence," 1982.

[43] G. Sperka, "Crystal growth in gels-a survey," Austria, 1988.

[44] M. Yoshimura and K. Byrappa, "Hydrothermal processing of materials: Past, present and future," in Journal of Materials Science, 2008 pp. 2085–2103.

[45] G. Will, "Powder diffraction: The Rietveld method and the two-stage method to determine and refine crystal structures from powder diffraction data, Springer Sciences and Business Media," 2006.

[46] M. Ermrich and D. Opper, Getting acquainted with the principles XRD for the analyst. 2011. [Online]. Available: www.panalytical.de

[47] C. L. Putzig et al., "Infrared Spectroscopy," 1994.

[48] L. M. Ng and R. Simmons, "Infrared spectroscopy," Anal Chem, vol. 71, no. 12, Jun. 1999.

[49] Ph. D. C. P. Sherman Hsu, "Infrared spectroscopy, Hand book of instrumental techniques for analytical chemistry," pp. 247–283.

[50] Robert W Silverstein and G. Clayton Bassler, "Spectrometric identification of organic compounds," p. 553, 1962.

[51] N. Saadatkhah et al., "Experimental methods in chemical engineering: Thermogravimetric analysis—TGA," 2020.

[52] J. D. Menczel and R. Bruce. Prime, Thermal analysis of polymers. John Wiley, 2009.

[53] S. Weisenburger and V. Sandoghdar, "Light microscopy: an ongoing contemporary revolution," Contemp Phys, vol. 56, pp. 123–143, 2015.

[54] H. T. Flakus and M. Chelmecki, "Infrared spectra of the hydrogen bond in benzoic acid crystals: Temperature and polarization effects, Acta - Part A Mol. Biomol. Spectrosc," vol. 58, no. 1, pp. 179–196, 2001.

Bibliographic References

[55] S. W. J. L. F. G. and A. K. F. Krichen, “Design of lanthanide metal organic frameworks incorporating dicarboxylate ligands, J. Porous Mater, vol. 26, no. 6,” pp. 1679–1689, 2019.

[56] Y. F. Zhou, F. L. Jiang, Y. Xu, R. Cao, and M. C. Hong, “Two-dimensional lanthanide Isophthalate coordination polymers containing right - and left - handed helical chains,” J Mol Struct, vol. 691, pp. 191–195, 2004.

[57] Y. Qu, Y. Ke, S. Lu, R. Fan, G. Pan, and J. Li, “Hydrothermal synthesis, structures and spectroscopy of 2D lanthanide coordination polymers built from helical chains: [Ln2(BDC) 3(H2O)2]n (Ln=Sm, 1; Ln=Eu, 2; BDC=1,3-benzenedicarboxylate),” J Mol Struct, vol. 734, no. 1–3, pp. 7–13, Jan. 2005, doi: 10.1016/j.molstruc.2004.03.035.

[58] L. Q. Fan and J. H. Wu, “Poly[diaqua-tris(μ4-isophthalato) dilanthanum (III)],” Acta Crystallogr Sect E Struct Rep Online, vol. 66, no. 2, 2010, doi: 10.1107/S1600536809054543.

[59] R. H. Zeng, “Poly [diaqua tris (4-benzene-1,3-di-carboxyl-ato) diterbium (III)],” Acta Crystallogr Sect E Struct Rep Online, vol. 63, no. 12, Nov. 2007.

[60] P. Mahata, K. V Ramya, and S. Natarajan, “Supplementary Material (ESI) for Synthesis, Structure and Optical Properties of Rare-Earth Benzene Carboxylates,” 2007.

[61] D. X. Hu, P. K. Chen, F. Luo, Y. X. Che, and J. M. Zheng, “Hydrothermal synthesis, structure and properties of two lanthanide benzene dicarboxylate, possessing infinite Ln-O-Ln linkages,” J. Mol. Struct, vol. 837, no. 1–3, pp. 179–184, 2007.

[62] C. Song et al., “Construction of Three New Lanthanide-Organic Frameworks with (3,6)-Connected rtl -Type Topology,” Synthesis and Reactivity in Inorganic, Metal-Organic and Nano-Metal Chemistry, vol. 46, no. 8, pp. 1174–1178, 2016.

[63] L. P. Zhang, Y. H. Wan, and L. P. Jin, “Hydrothermal synthesis and crystal structure of neodymium (III) coordination polymers with isophthalic acid and 1,10-phenanthroline,” Polyhedron, vol. 22, no. 7, pp. 981–987, 2003.

[64] P. Mahata, K. V. Ramya, and S. Natarajan, “Synthesis, structure and optical properties of rare-earth benzene carboxylates,” Dalton Transactions, no. 36, pp. 4017–4026, 2007.

Bibliographic References

[65] P. Wang, R. Fan, Y. Yang, X. Liu, W. Cao, and B. Yang, "Synthesis, crystal structures and properties of lanthanide-organic frameworks-based benzene carboxylates with two/three-dimensional structure," J Solid State Chem, vol. 196, pp. 441–450, 2012.

[66] R. S. Zhou, X. B. Cui, J. F. Song, X. Y. Xu, J. Q. Xu, and T. G. Wang, "Syntheses, structures and luminescence properties of lanthanide coordination polymers with helical character," J Solid State Chem, vol. 181, pp. 2099–2107, 2008.

[67] C. Daiguebonne, N. Kerbellec, Y. Gérault, and O. Guillou, "A new family of luminescent lanthanide-based coordination polymers," J Alloys Compd, vol. 451, pp. 372–376, 2008.

[68] A. De Betiencourt-Dias, "Isophthalato-based 2D coordination polymers of Eu (III), Gd (III), and Tb (III): Enhancement of the terbium-centered luminescence through thiophene derivatization," Inorg Chem, vol. 44, pp. 2734–2741, 2005.

[69] H. Flemig, I. Pantenburg, and G. Meyer, "Selten-erd-metall-koordinationspolymere: Synthesen und kristallstrukturen von sechs neuen pimelinaten," Z Anorg Allg Chem, vol. 632, no. 14, pp. 2205–2208, 2006.

[70] A. Dimos et al., "Microporous rare earth coordination polymers: Effect of lanthanide contraction on crystal architecture and porosity," Chemistry of Materials, vol. 14, no. 6, pp. 2616–2622, 2002.

[71] L. Yang, L. Liu, L. Wu, H. Zhang, and S. Song, "A series of 3D isomorphous lanthanide coordination polymers based on flexible dicarboxylate ligand: Synthesis, structure, characterization, and properties," Dyes and Pigments, vol. 105, pp. 180–191, 2014.

[72] H. T. Flakus and A. Miros, "Infrared spectra of the hydrogen bond in pimelic acid crystals: polarization and temperature effects," 2001. [Online]. Available: www.elsevier.com/locate/saa

[73] E. San Sebastian, "Coordination chemistry Group design, synthesis and characterisation of multifunctional MOFS from gas adsorption and photocatalysis to ciss effect and spin," Uxua Huizi Rayo, 2020.

[74] M. A. Halcrow, "The effect of ligand design on metal ion spin state-lessons from spin crossover complexes," 2016, United Kingdom.

Bibliographic References

[75] X. Li, Y. Bin Zhang, and Y. Q. Zou, "Hydrothermal synthesis, crystal structure, and luminescence of lanthanide (III) coordination polymers with tetrafluoro succinate and 1,10-phenanthroline," J. Mol. Struct, vol. 919, no. 1–3, pp. 277–283, 2009.

[76] A. N. Gusev et al., "Synthesis, structure and luminescence studies of Eu (III), Tb (III), Sm (III), Dy (III) cationic complexes with acetylacetone and bis(5-(pyridine-2-yl)-1, 2, 4-triazol-3-yl) propane," Inorganica Chim Acta, vol. 406, pp. 279–284, 2013.

[77] J. F. Chen et al, "'Two-dimensional dysprosium (III) coordination polymer: Structure, single-molecule magnetic behaviour, proton conduction, and luminescence,' Front.," vol. 10, p. 974914, 2022.

[78] M. Kariem, M. Kumar, M. Yawer, and H. N. Sheikh, "Solvothermal synthesis and structure of coordination polymers of Nd (III) and Dy (III) with rigid isophthalic acid derivatives and flexible adipic acid," J. Mol. Struct, vol. 1150, pp. 438–446, 2017.

Abstract

This manuscript presents the successful synthesis and characterization of seven series of coordination polymers constructed from lanthanide ions in combination with isophthalic acid and pimelic acid as organic linkers. Among the synthesized compounds, four series (Series 1–4) are newly reported compounds that, to the best of our knowledge, have not previously appeared in the literature. The remaining series (Series 5–7) correspond to known structures obtained with different lanthanide ions.

Comprehensive characterization was carried out using infrared (IR) spectroscopy, powder X-ray diffraction (PXRD), and thermal analysis. IR spectroscopy confirmed the coordination of isophthalate and pimelate ligands to the metal centers. PXRD analyses revealed the isostructurality, phase purity, and crystallinity of the synthesized compounds, while thermal studies demonstrated their multi-step decomposition behaviour.

Photoluminescence studies conducted in the visible range on selected compounds showed promising emission properties, highlighting their potential use in optical or sensing applications. The findings contribute to the growing body of knowledge on lanthanide-based coordination polymers and their functional properties.

Résumé

Ce travail présente la synthèse et la caractérisation réussies de sept séries de polymères de coordination obtenus à partir d'ions lanthanides associés à l'acide isophtalique et à l'acide pimélique comme ligands organiques. Parmi les matériaux synthétisés, quatre séries (séries 1 à 4) correspondent à de nouveaux composés, jamais rapportés dans la littérature. Les trois autres séries (séries 5 à 7) sont quant à elles déjà connues, mais obtenues ici avec d'autres ions lanthanides.

La caractérisation des composés a été réalisée par spectroscopie infrarouge (IR), diffraction des rayons X sur poudre (DRX) et analyse thermique. La spectroscopie IR a confirmé la coordination des ligands isophtalate et pimélate aux centres métalliques. Les analyses PXRD ont permis de démontrer l'isostructuralité, la pureté de phase et la cristallinité des composés. Les analyses thermiques ont révélé une décomposition en plusieurs étapes.

Le comportement photoluminescent de certains composés a été étudié dans le domaine du visible. Plusieurs d'entre eux ont montré des propriétés d'émission prometteuses, suggérant leur potentiel dans des applications optiques ou de détection.